AN INTEGRATED IMAGING SENSOR FOR RARE CELL DETECTION APPLICATIONS

A THESIS SUBMITTED TO
THE GRADUATE SCHOOL OF NATURAL AND APPLIED SCIENCES
OF
MIDDLE EAST TECHNICAL UNIVERSITY

BY

ÇAĞLAR ALTINER

IN PARTIAL FULLFILLMENT OF THE REQUIREMENTS
FOR
THE DEGREE OF MASTER OF SCIENCE
IN
MICRO AND NANOTECHNOLOGY

NOVEMBER 2012

Approval of the thesis:

AN INTEGRATED IMAGING SENSOR FOR RARE CELL DETECTION APPLICATIONS

submitted by **ÇAĞLAR ALTINER** in partial fulfillment of the requirements for the degree of **Master of Science in Micro and Nanotechnology Department, Middle East Technical University** by,

Prof. Dr. Canan Özgen
Dean, Graduate School of **Natural and Applied Sciences** _____

Prof. Dr. Mürvet Volkan
Head of Department, **Micro and Nanotechnology** _____

Prof. Dr. Tayfun Akın
Supervisor, **Electrical and Electronics Eng. Dept., METU** _____

Dr. Selim Eminoğlu
Co-Supervisor, **Mikro-Tasarım San. ve Tic. Ltd. Şti.** _____

Examining Committee Members:

Assoc. Prof. Dr. Haluk Külah
Electrical and Electronics Eng. Dept., METU _____

Prof. Dr. Tayfun Akın
Electrical and Electronics Eng. Dept., METU _____

Dr. Selim Eminoğlu
Mikro-Tasarım San. ve Tic. Ltd. Şti. _____

Dr. Ebru Özgür
MEMS Research and Application Center, METU _____

Assoc. Prof. Dr. Uğur Tamer
Pharmacy Department, Gazi University _____

Date: 28.11.2012

I hereby declare that all information in this document has been obtained and presented in accordance with academic rules and ethical conduct. I also declare that, as required by these rules and conduct, I have fully cited and referenced all material and results that are not original to this work.

Name, Last Name: Çağlar ALTINER

Signature:

ABSTRACT

AN INTEGRATED IMAGING SENSOR FOR RARE CELL DETECTION APPLICATIONS

Altıner, Çağlar

M.Sc., Micro and Nanotechnology Department

Supervisor : Prof. Dr. Tayfun Akın

Co-Supervisor : Dr. Selim Eminoğlu

November 2012, 75 pages

Cell detection using image sensors is a novel and promising technique that can be used for diagnostic applications in medicine. For this purpose, cell detection studies with shadowing method are performed with yeast cells (*Saccharomyces cerevisiae*) using an 32×32 complementary metal oxide semiconductor (CMOS) image sensor that is sensitive to optical illumination. Cells that are placed zero distance from the sensor surface are detected using the image sensor which is illuminated with four fixed leds to maintain fixed illumination levels in each test. Cells are transferred to the sensor surface with drying the medium they are in, which is phosphate buffered saline (PBS) solution. Yeast cells that are zero distance from the surface are detected with a detection rate of 72%. Then, MCF-7 (breast cancer) cells are detected with the same sensor when the PBS solution is about to dry. To investigate the detection capability of the sensor while the cells are in the PBS solution, the sensor surface is coated with gold

in order to immobilize the surface with antibodies. With immobilizing antibodies, cells are thought to be bound to the surface achieving zero distance to the sensor surface. After coating gold, antibodies are immobilized, and same tests are done with MCF-7 cells. In the PBS solution, no sufficient results are obtained with the shadowing technique, but sufficient results are obtained when the solution is about to dry.

After achieving cell detection with the image sensor, a similar but large format image sensor is designed. The designed CMOS image sensor has 160×128 pixel array with 15µm pitch. The pixel readout allows capacitive and optical detection. Thus, both DNA and cell detection are possible with this image sensor. The rolling line shutter mode is added for reducing further leakage at pixel readout. Addressing can be done which means specific array points can be investigated, and also array format can be changed for different size cells. The frame rate of the sensor can be adjusted allowing the detection of the fast moving cell samples. All the digital inputs of the sensor can be adjusted manually for the sake of flexibility. A large number of cells can be detected with using this image sensor due to its large format.

Keywords: rare cell detection, CMOS image sensor

ÖZ

HÜCRE TESPİTİ UYGULAMALARI İÇİN ENTEGRE GÖRÜNTÜLEME SENSÖRÜ

Altıner, Çağlar

Yüksek Lisans, Mikro ve Nanoteknoloji Bölümü

Tez Yöneticisi : Prof. Dr. Tayfun Akın

Ortak Tez Yöneticisi : Dr. Selim Eminoğlu

Kasım 2012, 75 sayfa

Görüntü sensörü kullanılarak hucre algılama, tıpta teşhis uygulamaları için kullanılabilecek yeni ve gelecek vaat eden bir tekniktir. Bu amaç için, gölgelendirme metoduyla yapılan hücre tespit çalışmaları; optik aydınlatmaya duyarlı, 32×32 tamamlayıcı yarı-iletken metal oksit (CMOS) görüntü sensörü kullanılarak maya hücreleri (*Saccharomyces cerevisiae*) ile gerçekleştirildi. Sensör yüzeyinden sıfır mesafeye yerleştirilen hücreler, her testte aynı aydınlatma seviyesini korumak amacıyla yerleştirilen dört sabit led ile aydınlatılan görüntü sensörü aracılığıyla tespit edildi. Hücreler, sensör alanına fosfat tamponlu tuz (PBS) çözeltisinin kurutulmasıyla aktarıldı. Sensör yüzeyinden sıfır mesafede konumlandırılan maya hücreleri %72 başarıyla algılandı. Sonra, MCF-7 (meme kanseri) hücreleri, aynı sensör ile PBS çözeltisi kurumak üzereyken algılandı. Sensörün hücreler PBS çözeltisi içindeyken algılama kabiliyetini araştırmak amacıyla yüzey alanı, altınla kaplandı ve altın yüzeylere antikorlar

tutunduruldu. Böylelikle hücrelerin sensör yüzeyine sıfır mesafede olması sağlandı. Aynı testler bu sensörde tekrarlandı ve gölgelendirme metodu ile PBS çözeltisi içerisinde başarılı algılama gerçekleştirilemedi fakat, çözelti kurumak üzereyken başarılı algılama sonuçları elde edildi.

Görüntü sensörü ile hücre algılaması sağlanmasıyla, benzer ama geniş formatlı bir görüntüleme sensörü tasarlanmıştır. Tasarlanan CMOS görüntüleme sensörü 160×128 formatındadır ve 15µm büyüklüğünde piksellerden oluşmaktadır. Piksel okuma devresi kapasitif ve optik algılamaya uygun tasarlanmıştır. Böylelikle tasarlanan görüntüleme sensörü, hem DNA hem de hücre algılama uygulamalarını mümkün kılar. Pikseldeki kaçak akımı daha aza indirgemek için sensöre yuvarlanan hat çekim modu eklenmiştir. Spesifik alanların incelenebilmesi ve dizin formatının, farklı boyutlardaki hücreleri tespit edebilmesi amacıyla değiştirilebilmesi için adresleme yapılabilir. Sensörün çerçeve hızı, hızlı hareket eden hücre örneklerinin tespiti için ayarlanabilir. Esneklik sağlaması açısından, sensörün bütün dijital girişlerinin manuel bir şekilde ayarlanabilmesi sağlanmıştır. Formatı büyük olduğundan, çok sayıda hücre, bu görüntü sensörü kullanılarak tespit edilebilir.

Anahtar kelimeler: nadir görülen hücre algılama, CMOS görüntüleme sensörü

To my beloved father

ACKNOWLEDGEMENTS

I would like to thank my advisors Prof. Dr. Tayfun Akın and Dr. Selim Eminoğlu for their supervision and guidance, both in academic and professional career.

I would like to thank Assoc. Prof. Dr. Haluk Külah for giving opportunity for the cell detection tests, and also his advices during this period.

I would like to thank Dr. Yusuf Tanrıkulu for his helps in the clean room about screening the sensor samples with SEM. Also, I would like to thank Dr. Murat Tepegöz for sharing his experiences with me.

I would like to thank Dr. Yekbun Adıgüzel for her guidance and help with the cell detection tests, and preparing the material for these tests. Also, I would like to thank Cavid Musayev for his helps with the cell detection test setup and sensor preparation.

I would like to thank Murat Erdem for preparing cancer cells for cell detection tests.

I would like to thank Metehan Erdoğan for helping me with the electroless gold plating process.

Thanks to all my colleagues at Mikro-Tasarım for their precious help and advices during the whole thesis process.

I would like to thank my mother, Şenol Altıner, for her support and encouragement during my whole life.

Finally, I would like to thank my love, Seda Tutluer, for her encouragement and support in all of the areas of my life.

TABLE OF CONTENTS

LIST OF TABLES

TABLES

LIST OF FIGURES

FIGURES

CHAPTER I

INTRODUCTION

Cell is the smallest building block of living organisms. Detecting cells, even rare cells, is more evident in the beginning of 1980s with the detection and isolation of rare fetal cells which is triggered by the invention of polymerase chain reaction (PCR) [1]. Following this study, cell detection researches reach to the point that will be useful for diagnosing some specific diseases with detecting rare cells in specific samples. Not only the researchers found carcinogenic diseases, but also achieve to detect unnecessary harmful substances in the body with the help of rare cell detection techniques. Similar to these techniques, DNA detection applications are also helpful for diagnosing diseases. In this technique, problematic DNA strands are defined and detected as a part of the treatment. DNA detection is also needed for early diagnosis of some cancer types.

This thesis describes a technique for cell detection applications with the help of electronics. An integrated imaging sensor is used for the detection. The detailed analysis and operating principles will be explained. Since an imaging sensor will be used, photonic beams reaching to the sensor coming from the samples will be detected. Shadows of the cells formed by the fixed light sources are examined using an image sensor. Characteristic beams coming from the sample can also be obtained by giving characteristic light to the sample. This sensor is not designed for a specific cell detection application, so according to the sensor architecture, various possible detection applications will be mentioned.

This chapter gives a brief introduction to both biomedical and electronics parts of the thesis. Section 1.1 explains how the related studies detect cells in the literature. Section 1.2 describes the readout electronics in these studies. Section 1.3 gives information about the readout technique used in this study. Lastly, Section 1.5 describes research objectives of the thesis and thesis organization.

1.1 Electronics Use in Cell Detection Applications

There are several techniques about cell detection applications. These techniques can include chemistry, optics, mechanics, electronics separately or combination of some of these disciplines [2]. Very good examples of combination of these disciplines can be given with BioMEMS chips which use dielectrophoresis technique. Dielectrophoresis technique is about exerting forces to the charged or uncharged molecules in the existence of an applied electric field [2]. With the help of this technique, people succeeded in rare cell population analysis and detection, or even manipulated the desired individual cells without giving damage to the viability of them [3-4].

Detection of the neural or cardiac activity is another application of this subject. Studies are carried out for the detection of cells which are responsible for creating action potentials in neural network or in cardiac network. With the help of this technique, neural and cardiac maps of human body are generated, and the irregularities and problems can be detected [5-6].

Another application area is about the DNA detection techniques. DNA detection shows similarities with the rare cell detection by means of detecting specific less found amounts of materials in the sample. In the literature, there are numerous DNA detection techniques including impedance based, phosphate backbone based or charge based. In impedance based DNA detection technique, impedance change between electrodes due to DNA hybridization is measured [7]. In phosphate backbone based DNA detection technique, hybridization of DNA drives a change in the number of ions in the solution, and some ion sensitive transistors sense this change [8]. All these detection techniques rely on the specific, wanted DNA strands' hybridization. In other

words, if there is a strand that is sought or not sought, the hybridization occurs or not and the required strand will be detected. Similar study is worked out in METUMEMS group with the charge based detection technique [9]. In this technique, if the desired DNA strand is hybridized with the immobilized counterpart, electrons release, and these electrons are read out by some electronics behind.

Projection of shadow image patterns into the image sensors is very popular because of its several advantages. Figure 1.1 shows cross sectional view of CMOS sensor fabricated with well chamber. Distances between the well chamber and the sensor surface are (a) 0µm, (b) 25µm, and (c) 685µm. Since it is a lens free application and does not require any mechanical or optical scanning environment, the system is compact. Thus, this technique is a cost effective cell detection technique. In this technique, labeled cells are introduced to a well chamber which is placed on top of a commercially available image sensor [10]. Well chamber to sensor distance is arranged to three different positions in order to observe the effect of cell distance to the sensor.

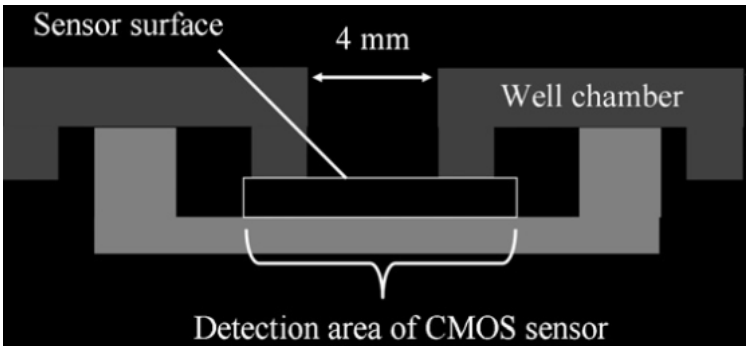

(a)

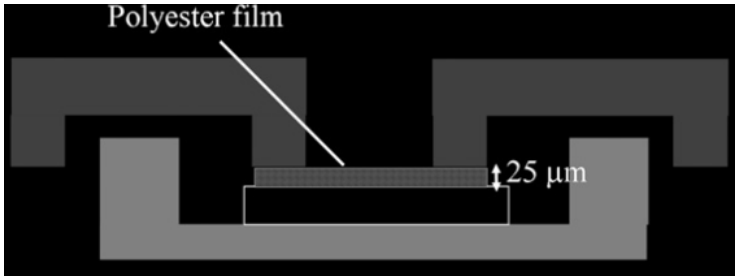

(b)

Figure 1.1: Cross sectional view of CMOS sensor fabricated with well chamber. Distances between the well chamber and the sensor surface are (a) 0µm, (b) 25µm, and (c) 685µm.

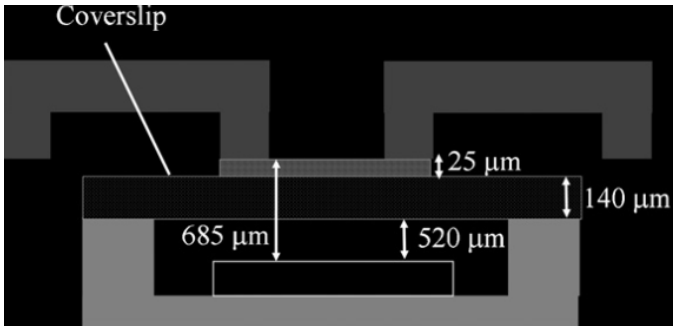

(c)

Figure 1.1: cont'd

Figure 1.2 shows CMOS sensor images of various sizes of microparticles under different separation distances between particles and sensor surface [10]. There is no external light source used for detecting cells, instead of that chemiluminescent imaging. This is done by labeling the micro-particles and HeLa cells on CMOS image sensor. Three different sized cells and particles are used for observing the differences of images taken from the sensor.

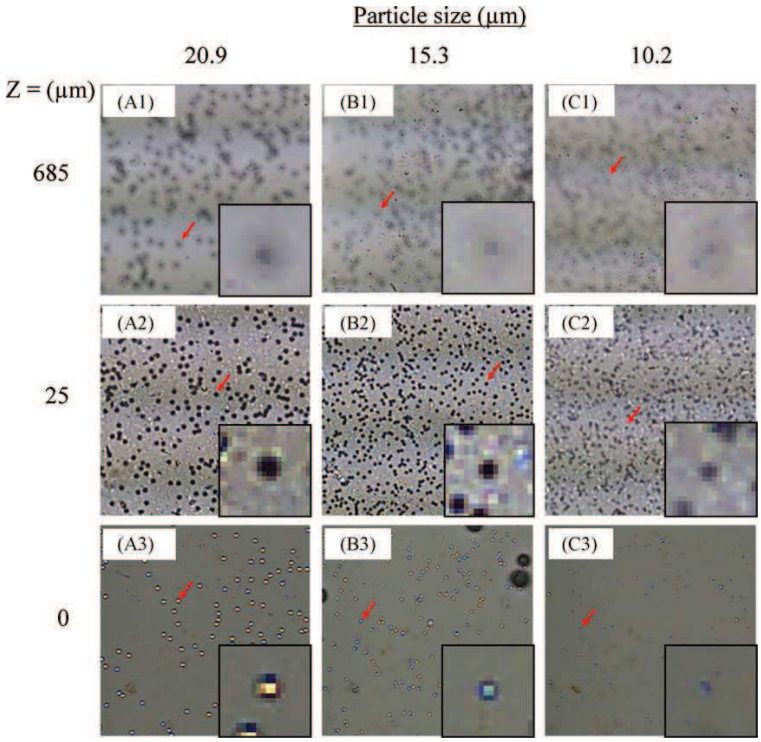

Figure 1.2: CMOS sensor images of various sizes of micro-particles (A-C) under different separation distances between particles and sensor surface (1-3) [10].

There are several conclusions about the study. The first conclusion is that the images taken with the particle distance, 685µm, are unclear as can be seen at the top row. Second conclusion is that the images taken with the particle distance 25µm above the sensor are seen as black spots, and they are slightly enlarged images because of the shadowing effect. The last and the most interesting conclusion is obtained with the particles that are placed directly onto the sensor. The images of the particles are brighter than the background image. The reason is said to be the lens effect that is, the light has been focused to the sensor array by the particles.

Figure 1.3 shows CMOS sensor and microscopic images of HeLa cells without and with heat treatment after trypan blue staining [10]. The brighter image is seen in HeLa cells too. Additionaly, the blue stained cells with the help of heat treatment is also seen as blue using CMOS image sensor.

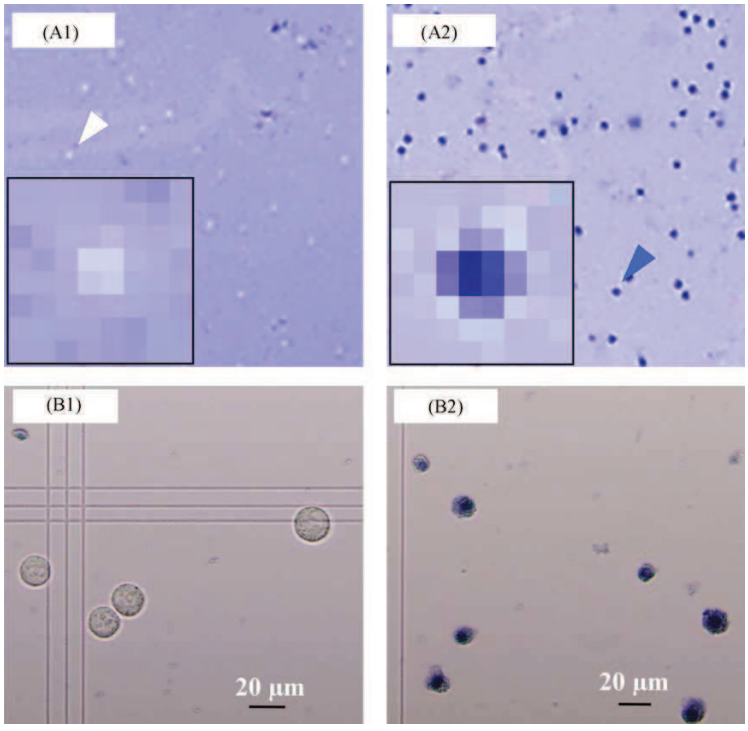

Figure 1.3: CMOS sensor (A) and microscopic (B) images of HeLa cells without (A1 and B1) and with (A2 and B2) heat treatment after trypan blue staining [10].

This technique is used to detect bacteria cells [11] or monocytes, NIH-3T3 fibroblasts, mESCs and red blood cells [12]. In all these studies, it is seen that the shadowing effect works for detecting cells. The distance between the cells and the sensor is changed for observing the effect of it, and also effect of the diameter of the cells are investigated in these studies. This shadowing technique is also used for size categorization of the detected cells [13]. The velocity of these particles is also measured in the same study with using two identical sensor arrays.

The last detection technique uses both optics and electronics. This technique basically uses optical signals coming from the samples which are excited externally, and detects these signals with the help of some sensors and electronics. The coming signals to the sensors including information about the samples' ingredient and rare cell detection will be realized.

Related to this subject, there are two main imaging methods carried out with the ultraviolet (UV) wavelength signals. First one is reflected UV imaging, and the second one is fluorescence UV imaging. In the reflected UV imaging method, UV signal is introduced to the sample, and the reflected signals coming from the sample is detected. In the fluorescence UV imaging, again UV signal is exposed to the sample, and detected signals come from the samples' re-excitation. These re-excited signals are usually at different wavelengths from the incoming UV signal, and these different wavelengths are usually in the visible or near-UV range. The advantage of this method is that visible sensors can be used in order to detect these signals [14].

In this thesis, one of the main methods that is used for rare cell detection is fluorescence UV imaging method. In this method, as mentioned above, emission from the sample due to the initial excitation is detected. This emission is occurred due to some interactions which takes place in the tissue (sample).

In the tissue, there are several interactions that include scattering, absorption, fluorescence emission etc. [15]. Figure 1.4 shows light-tissue interactions including reflectance, scattering, absorption, and fluorescence. Fluorescence UV imaging is interested in fluorescence emission of this interaction.

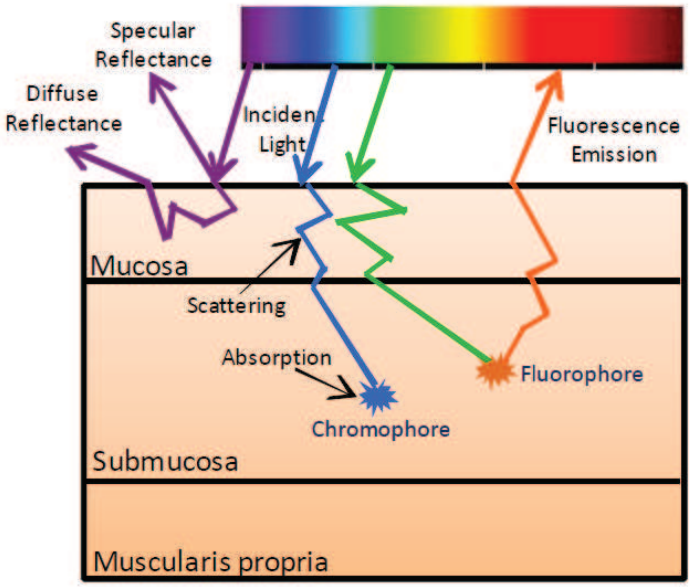

Figure 1.4: Light-tissue interactions including reflectance, scattering, absorption, and fluorescence [15].

Fluorescence emission is due to the excitation of fluorophores in the tissue. There are quite a number of fluorophores which are in fact aromatic amino acids present in the cells. Some of these fluorophores are tryptophan and tyrosine; and some related coenzymes NADH and NADPH [15]. Each of these fluorophores emits at different wavelengths when excited at specific wavelengths. Table 1.1 shows excitation and emission maxima of some endogenous fluorophores.

Table 1.1: Excitation and emission maxima of some endogenous fluorophores [15].

Endogenous fluorophores	Excitation maxima (nm)	Emission maxima (nm)
Amino acids		
Tryptophan	280	350
Tyrosine	275	300
Phenylalanine	260	280
Metabolic cofactors		
FAD, Flavins	450	515
NADH	350	450
NADPH	336	464

Figure 1.5 shows fluorescence behavior representation (mean spectra) of some colorectal tissues. All of the endogenous fluorophores exist in the submucosa layer of the tissue. To excite fluorophores, the incoming light has to penetrate down to the submucosa layer from mucosa layer. In neoplastic tissues (tissues formed with tumors), haemoglobin (Hb) concentration is higher. The higher Hb concentration do not allow incoming light pass through mucosa to submucosa resulting fluorescence emission. So, in the presence of cancer tissues, the emitted light intensity coming from the tissue is weaker compared to the normal tissue [16].

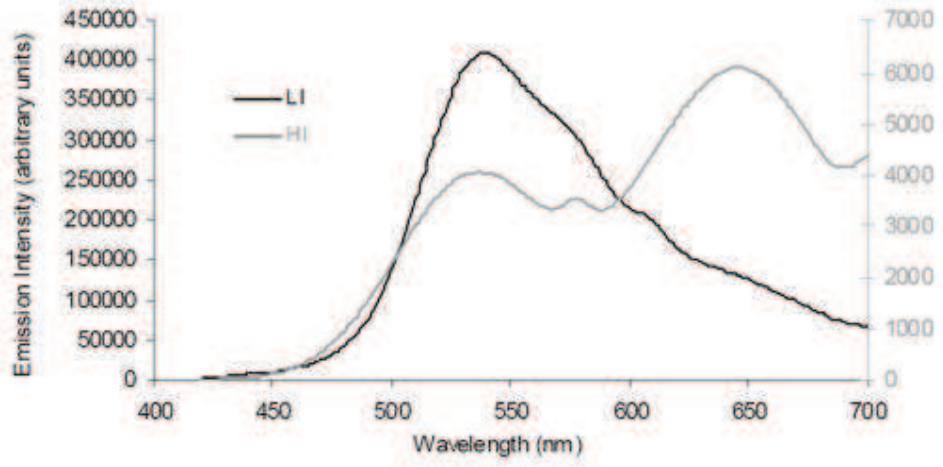

Figure 1.5: Fluorescence behavior representation (mean spectra) of some colorectal tissues [16].

This behavior is obtained from the excitation of the epithelial tissues at around 400nm to 550nm. It can be understood from Figure 1.5 that fluorescence emission is higher in normal tissue than neoplastic tissue at wavelength around 515nm [17]. If the sensor is designed to have higher quantum efficiencies at these wavelengths, early cancer diagnosis is succeeded.

Designed sensor must be sensitive to the required specific wavelengths in order to detect the right signals. The absorption of light by the silicon sensor is another issue to be deal with. Emitted light coming from the tissue is not always directly exposed to the photosensitive material of the sensor. Over the photosensitive materials, there are

usually passivation layers that protect sensors from the external threats. Different layers are also laid between the metal layers of the sensor in order to separate each of them. These layers are usually composed of oxide layers. These oxide layers determine the transmittance of light coming to the sensor.

Figure 1.6 shows simulated spectral responses of some typical combinations of the dielectric layers above the photodiode pn-junction. There is nearly a certain transmittance percentage when no dielectric layer is used. With using dielectric layers, wavelength dependency occurs. More dielectric layer usage brings highly oscillated transmittance percentage but also increases transmittance at some wavelengths. It is very hard to etch all dielectric layers above the photosensitive material because this process can damage the photodiode with giving roughness on it. So, people in [18] left one oxide layer on the photosensitive material for their application. Some filters also can be used in order to sense the specific wavelength of interest. Another solution for optimizing transmittance is using anti-reflective coating over the sensor but it requires some post-processing steps over standard CMOS process.

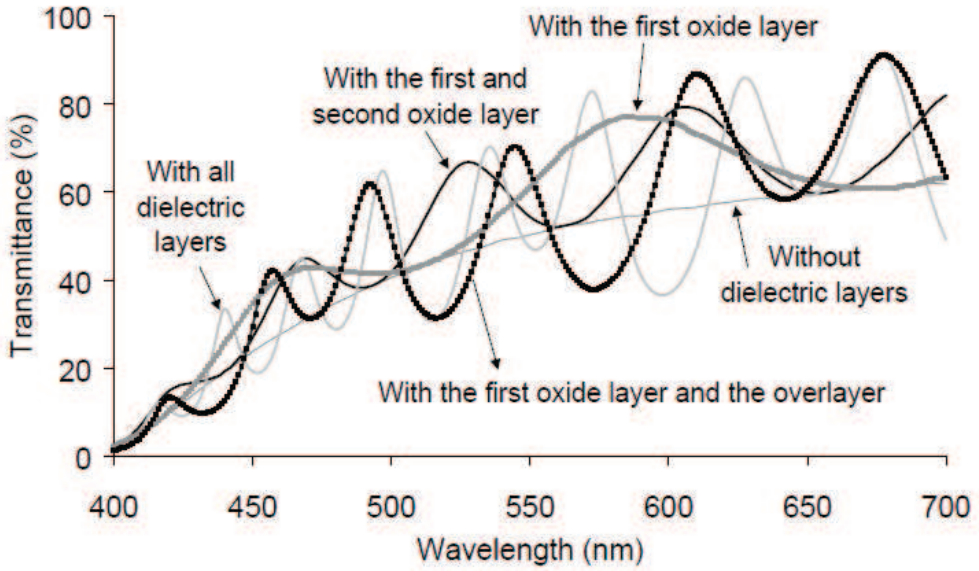

Figure 1.6: Simulated spectral responses of some typical combinations of the dielectric layers above the photodiode pn-junction [18].

The disadvantage of this solution is that post-processing increases the cost of the sensor. Another opportunity to optimize the spectral response of photosensitive material is changing the junction depth of it but again this is a costly process because of being not a standardized process.

The last example of these detection techniques is measuring uric acid in serum, plasma or cell. Figure 1.7 shows the macroscopic measurements of absorbance spectra for different uric acid concentrations. Decrease or increase in uric acid in human body causes disorders like leukemia, Wilson's disease etc. To detect abnormal uric acidic cells can prevent a person to suffer from these diseases. The principle is similar with the above examples. Samples with higher uric acid concentration absorb light more so intensity of light coming to the sensor directly shows the difference between different uric acid concentrated samples [19].

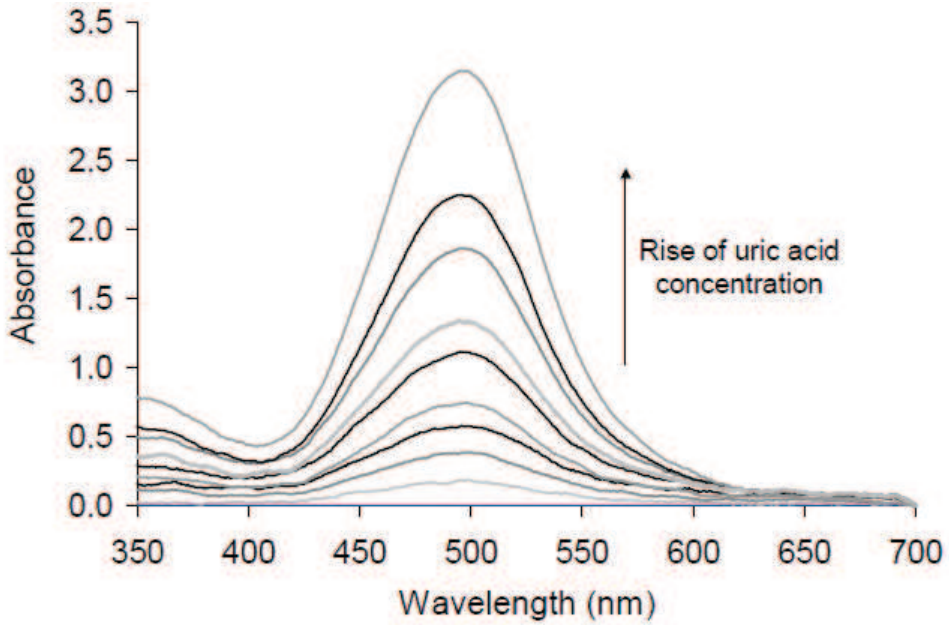

Figure 1.7: Macroscopic measurements of absorbance spectra for different uric acid concentrations. From bottom to top curve: 5, 10, 15, 20, 30, 40, 60, 80, and 120mg/dl [19].

The figure explains that, the peak absorbance wavelength is around 494nm so the designed sensor must be sensitive to this value. To detect this specific signal, optical filters should be placed on top of the sensor in addition to selecting the suitable oxide thicknesses explained above [19].

1.2 Readout Electronics in Rare Cell Detection Techniques

Identifying specific DNA strands is realized with the readout electronics. The sensor designed in METUMEMS senses the electrons that reveal as a result hybridization of DNA strands. The function of the sensor is to capture the electrons, and give this information to the outer world. Electrons, revealed on the sense node results a net charge. As a result of this charge, voltage on the sense node is buffered to the output. The critical point in this design is that even small number of electrons must be read out so the noise of the system is very important, and the noise is achieved in the range of seven electron levels [9].

The cell detection techniques mentioned in Section 1.1 are all about detecting the light emitted from the samples or reaching to the sensor surface from the source. Generally, these photons are detected with photosensitive diodes, preferably silicon based photodiodes because of their standardized and conventional processes. A photodiode is actually a diode, and its I-V characteristic is dependent of light illumination that it is exposed.

Figure 1.8 shows photodiode symbol with the characteristic curve [20]. In the applications used as a detector, these kind of diodes are used in the reverse bias region in these applications, and anode probe of the diode is connected to the lowest voltage in the circuit (i.e. V_D is negative). In the reverse bias, there is a small negative saturation or dark current flows from diode even if there is illumination or not. With the increasing illumination, reverse bias current begins to increase, and the total diode current is equivalent to

$$I_D = -I_{DARK} - I_{PHOTO} \tag{1.2.1}$$

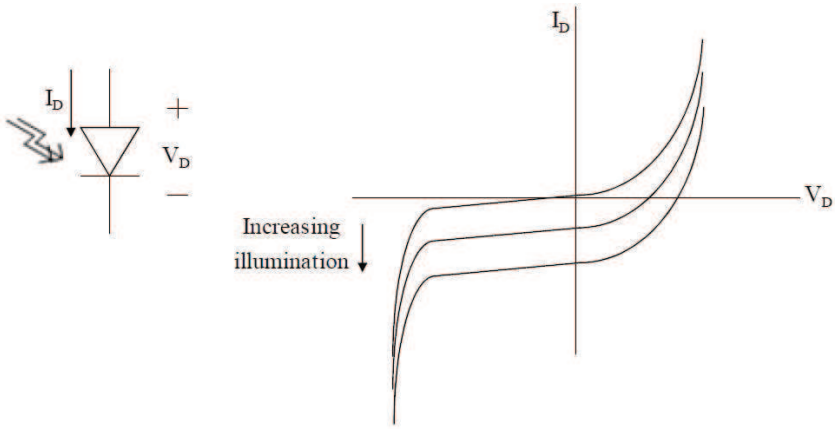

Figure 1.8: Photodiode symbol with the characteristic curve [20].

Figure 1.9 shows cross-section of a pn-junction photodiode. The increasing current leads to a voltage across the diode, and this voltage or charge on the diode is read out by some electronics behind it. Because of this voltage formation, the diode can be modeled as a capacitor.

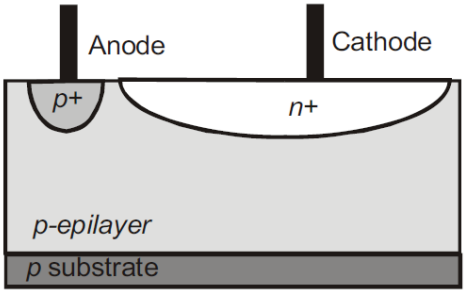

Figure 1.9: Cross-section of a pn-junction photodiode [17].

There several ways of reading this diode voltage. Generally, active pixel sensor topology is used for reading the photodiodes. Because of the reset noise of the source follower transistor correlated double sampling (CDS) is used for eliminating this noise.

CDS can be done either with a circuit in the sensor or out of the chip with some software.

Figure 1.10 shows readout diagrams of a CDS performing sensor. The voltage on PDC is transferred to APS_{out} node for CDS operation. Firstly, the reset voltage is stored on C_{rst} capacitor with srst signal. At the end of integration, output of the pixel voltage is stored on C_{sig} capacitor with ssig voltage. Finally, with coming en signal, voltage on C_{sig} capacitor is subtracted from voltage on C_{en} capacitor, and the result is buffered to a spatial filter circuit. Spatial filter block processes the output of CDS block, and makes the binary comparison of each pixel's voltage with the average voltage of all the pixels. Thus, every change for the coming light to the photodiodes results in change in the binary data of the spatial filter.

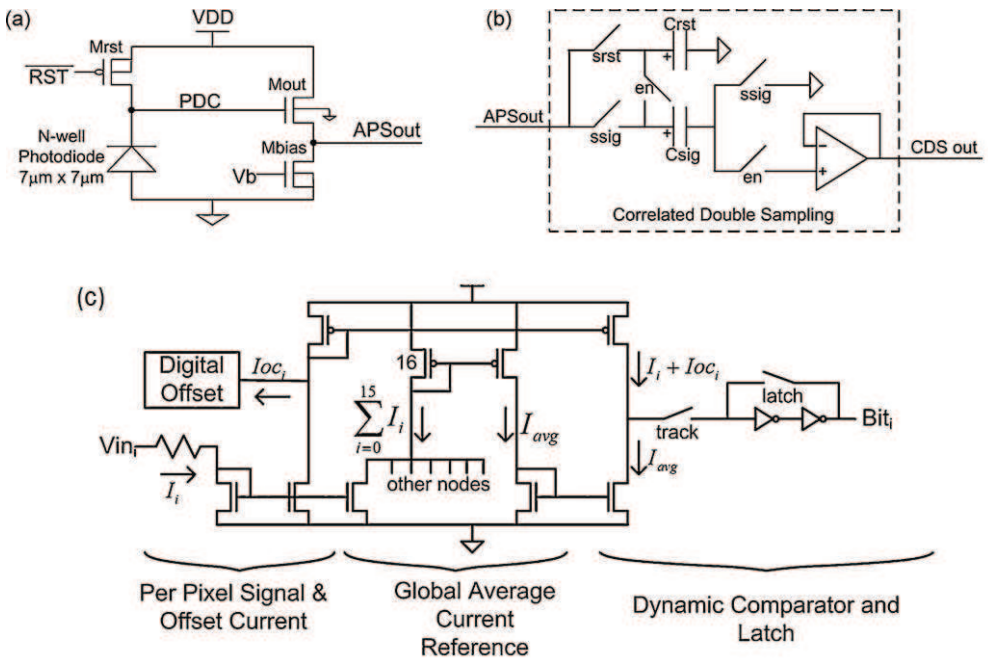

Figure 1.10: Readout diagrams of a CDS performing sensor. (a) Active pixel sensor topology (b) Correlated double sampling circuit (c) Schematic diagram of spatial filter and digital block performing serialization of the spatial filter's outputs [13].

Figure 1.11 and Figure 1.12 shows block diagram of the photodiode readout circuit, and comparator input and output voltages implemented in [18]. For the rare cell detection applications in [16-19], analog to digital conversion technique is used on the same die with the photodiodes. A comparator compares the photodiode voltage with a reference voltage, and produces a bit stream signal chain with the frequency proportional to the photocurrent which shows the intensity of light transmitted from the sample.

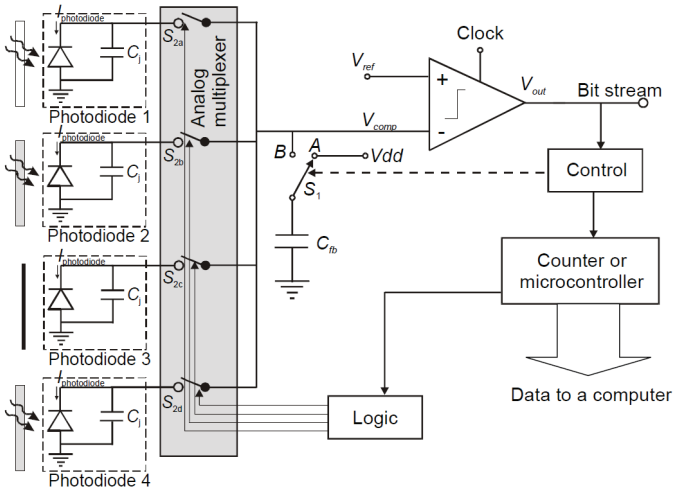

Figure 1.11: Block diagram of the photodiode readout circuit [18].

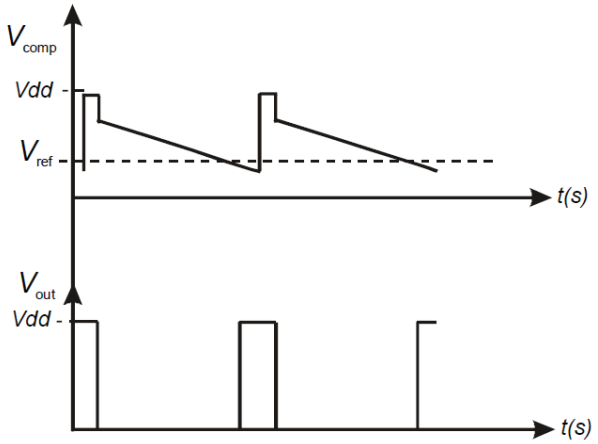

Figure 1.12: Comparator input and output voltages [18].

1.3 Active Pixel Sensor Readout Techniques

There are two types of CMOS pixel structures. First one is passive pixel structure, and this structure directly gives the diode voltage to the column with a switch behind it. No amplification or buffering circuitry is used in these kind of pixel structures. Second type is active pixel structure. Minimum three transistors are used in this type of pixels. A switch transistor is used to reset the diode voltage, another transistor is used for buffering, and a last transistor for giving the buffered voltage to the column bus. The advantage of these structures is that the diode voltage is not given directly to the column bus, and therefore charge sharing between the small diode capacitance, and the large bus capacitance is prevented. In active pixels, amplification of the input signal can also be done in the pixel level. There are several active pixel structures changing from three to several number of transistors in the literature.

The main goal of the active pixel readout circuit is to read the charge or voltage across the diode. In some applications, this voltage or charge on the diode can be read directly [9], while some of the techniques use amplification in the column level [21]. While reading the signal on the diode with any of these techniques, noise is the most problematic issue that must be cancelled. Reset noise generated by reset transistor and fixed pattern noise generated from column signal chain is the noise sources that can be cancelled by using a method called correlated double sampling [22]. In this method, pixel is read before and after reset operation. The difference of the outputs between two consecutive readings results in the noise free output of the system. This can be done with either on-chip readout methods or out of chip technique which the samples are differentiated externally by the help of software.

In this thesis, an active pixel sensor with a modified three transistor structure is used to read the photodiode. To eliminate reset noise or fixed pattern noise, out of chip CDS method is used.

1.4 Performance Parameters of Image Sensors

Performance of CMOS image sensors are evaluated by some parameters according to the application areas. In fact, there are two main parts of an image sensor. The detector detects the incoming photons, and generates electrons. The readout circuit behind the detector reads these electrons, and processes this information to give an output from the system.

In our case, the detector is a photodiode, and the function of the photodiode is to generate electrons from incoming photons but how many photons can reach to the photodiode? To answer this question, the beginning point is the illuminance (light level) parameter. The SI unit of illuminance is lux, and 1 lux is equal to 1.464 mW/m^2. To give an example, 1×10^4 lux illuminance level corresponds to the full daylight where 1lux approximately shows a full moon illuminance level at a clear night. 1 photon at 500nm wavelength (this value is taken into account for the calculations in this chapter because the wavelength value that is targeted to be detected with the image sensor is around this value) has an energy value in terms of W/sec

$$E = \frac{hc}{\lambda} = \frac{6.626 \times 10^{-34} \times 3 \times 10^{8}}{500 \times 10^{-9}} = 3.9756 \times 10^{-19}\, W.sec \tag{1.4.1}$$

where h is the Planck's constant, c is the speed of light, and λ is the wavelength. So, at 1lux illuminance of 500nm wavelength light, the number of photons falling to a unit meter square at 1 second is

$$@\ 1\ lux = \frac{0.001464}{3.9756 \times 10^{-19}} = 3.68 \times 10^{15}\ photons/sec.m^2 \tag{1.4.2}$$

Number of photons falling to a single photodiode area which is 4.7µm × 4.7µm is

$$\#\ of\ photons\ per\ diode\ = 3.68 \times 10^{15} \times (4.7 \times 10^{-6})^2 = 81345\ photons/sec \tag{1.4.3}$$

An important parameter for photon detectors is responsivity. Responsivity is defined as the output signal generated by received power and formulated by

$$R = \frac{I_P}{P_i} = \frac{q\eta\lambda}{hc} \tag{1.4.4}$$

where R is responsivity, I_P is photodiode current, P_i is received power, q is electron charge, η is quantum efficiency [17]. Quantum efficiency is defined as the electron hole pairs generated per incoming photon [23]. This value is process dependent, and cannot be optimized with a standard CMOS process. Here, the important point is the received power namely, received photons by the sensor. The calculated photon value in (1.4.3) is assumed that all the photons generated by the light source is received by the sensor. But as explained in Figure 1.6 not all the incident light is transmitted to the photodiode because of the oxide layers on it. There is a loss in the range of 50% has to be taken into account while calculating the incoming photons. Thus, number of incoming photons at 1 lux illumination at one second is about 40600 assuming the quantum efficiency is one. If quantum efficiency is taken approximately 50% like in [17-18], around 2×10^4 electrons are generated by single pixel in one second time interval.

In the readout side, there are also some performance parameters that determine the performance of the sensor. The most important parameter is noise associated with the readout. The dominant noise source is the reset noise generated on the diode capacitance due to the reset transistor in the pixel and equal to

$$Q_{reset} = \sqrt{kTC} \tag{1.4.5}$$

where k is the Boltzmann constant, T is the temperature, and C is the equivalent capacitor value of the photodiode. Here, noise in terms of charge is noted because the diode creates electrons, and the circuit reads the charge accumulated on the diode. The solution for cancelling this noise is the correlated double sampling method explained in Section 1.3. This is not the only noise source, and the noise generated by the readout circuit will be explained in the next chapter.

The capacitance value of the photodiode is calculated according to the foundry specified process parameters, and found approximately as 15fF. As stated above, 2×10^4 electrons generate voltage value on the diode as

$$V = \frac{Q}{C} = \frac{nq}{C} = \frac{2 \times 10^4 \times 1.6 \times 10^{-19}}{15 \times 10^{-15}} = 213mV \quad (1.4.6)$$

which means the readout must read around 213mV voltage differences in the photodiode according to the assumptions made in this section. Therefore, the noise level in the readout circuit must not prevent the readout from reading this voltage differences, and must be sufficiently less from this value.

1.5 Research Objectives of the Thesis and Thesis Organization

The first objective of the thesis is to test a CMOS image sensor with yeast cells if the image sensor is capable of detecting the cells with shadowing method explained in Section 1.1. Following the yeast cell tests, second aim is to detect cancer cells with binding them to antibodies using the same method. After the tests done by the image sensor, the second objective is to design a more advanced image sensor that will be used for rare cell detection applications again explained in Section 1.1.

The organization of the remaining part of the thesis is as follows:

Chapter 2 explains the working principle of the CMOS image sensor that is used for cell detection tests. The cell detection tests that are performed are also given in this chapter.

Chapter 3 is about the designed image sensor. Detailed explanation of each block of the image sensor is explained in this chapter.

Chapter 4 summarizes and concludes the thesis report. The future work will be included in this chapter.

CHAPTER II

CELL DETECTION TESTS

This chapter introduces the architecture of the image sensor that has been used for DNA detection and gives the related test results in the scope of a previous work [9]. Also, cell detection test results completed in the scope of this thesis work will be explained. The sensor was designed in METU-MEMS Research Group, and it is presented as a master thesis with the aim of detecting DNA strands. The DNA test results performed with the sensor in the scope of this previous master thesis will also be explained in this chapter. Another similar version of this sensor was designed for cell detection tests [9]. The differences of these two sensors will be explained, and the tests related with cell detection which are performed with this new version will be included in this chapter.

The organization of the chapter is as follows: Section 2.1 gives brief information about DNA detection studies obtained in previous work. Section 2.2 explains the new version of the sensor that is modified for cell detection tests, and electroless gold coating process applied on its activation surface. Section 2.3 gives the cell detection test results obtained with the modified sensor.

2.1 DNA Detection Studies Performed in a Previous Work

This section explains a previous master thesis work related with DNA detection study [9]. Section 2.1.1 describes the principle behind the CMOS image sensor that detects DNA strands. Section 2.1.2 shows the DNA detection test results obtained with the explained image sensor.

2.1.1 CMOS Image Sensor Used in DNA Detection Tests

Figure 2.1 shows the pixel structure of the chip. The image sensor used for DNA detection has 32×32 pixel array that has 15µm × 15µm area each.

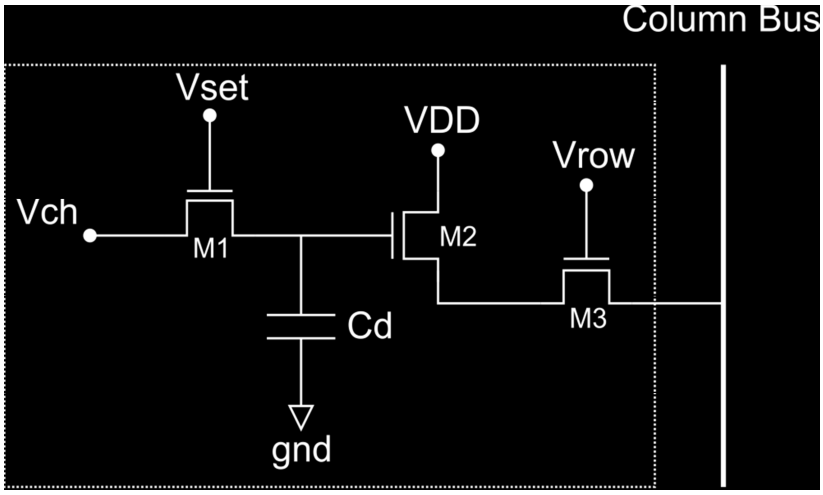

Figure 2.1: Pixel structure of the chip. M1 is the pixel reset switch, M2 is the pixel source follower, and M3 is the row switch transistor that transfers the pixel data to the column bus [9].

The data at the gate terminal of the M2 transistor is read by the circuit. There is no additional physical capacitor in the pixel. The capacitor in Figure 2.1 is only a representation of the total capacitance, and formed by gate to source capacitance of M2 and other parasitic capacitances.

Figure 2.2 shows top level illustration of the pixel. Detector material is the top metal connected to the gate terminal of M2 transistor. The aim of the sensor is to read the charge at this node. Immobilization of DNA strands occurs on top of this node with some post-processing. After the immobilization of DNA strands, their counterparts are exposed to the sensor for hybridization, and the charge accumulation on the sense node is read out by the sensor.

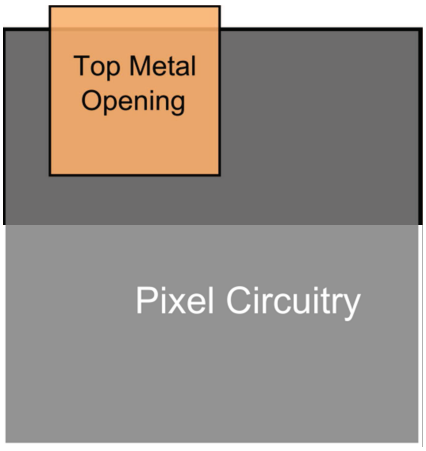

Figure 2.2: Top level illustration of the pixel structure [9].

Sense node is reset to a known voltage with M1 transistor, and read out first. After resetting, sample is exposed to the system, and charge due to hybridization, if exists, is read. If there is a charge drop, it means there is hybridization in the system, and DNA detection is realized.

The charge at the sense node is transferred to the column bus by M3 row switch transistor. In every column, there is a bias transistor that biases the M2 transistor for its proper operation. The current required for the bias transistor is given by a current mirror circuitry. The output is taken from a buffer that is connected to all of the bias transistors.

2.1.2 DNA Detection Test Results

DNA strands are exposed to the sensor in an ion contained buffer solution. Thus, detector metals of the sensor array must be isolated from each other. Figure 2.3 shows post CMOS surface modification and packaging of the chip. For isolation, nitride is coated on the sensor array. For immobilization of DNA strands, amino-propyl-triethoxy-silane (APTES) is covered on the sensor array. With this coating, a capacitive interaction occurs between the charges due to the immobilized DNA strands and detector top metal layer.

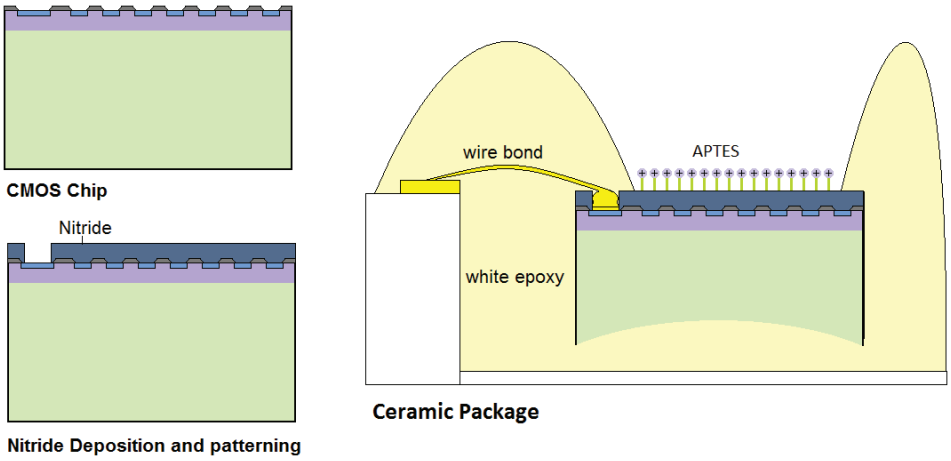

Figure 2.3: Post CMOS surface modification and packaging of the chip [9].

Sense node voltage of the sensor is read out by the sensor, and the output of the sensor is an analog signal. Output of the sensor is given to an analog-to-digital converter (ADC) chip. Leakage at the node voltage due to the capacitive interaction with DNA strands is calculated as ADC counts. So, ADC count means there is a net charge induced by the DNA strands.

Figure 2.4 shows the leakage values of some pixels in immobilization and hybridization case. Figure 2.4.(a) shows the immobilization leakage results for 5 pixels. Figure 2.4.(b) shows hybridization leakage result in a 1pM, 30uL target DNA solution. Figure 2.5 shows average leakage of pixels in performed tests. The immobilization ADC count (leakage value) is higher than the washed case which means the immobilized DNA strands are sensed by the sensor. Another result from Figure 2.5 is the hybridization ADC count value is higher than immobilization ADC count value which means the charges reveal as a result of hybridization is captured by the sensor.

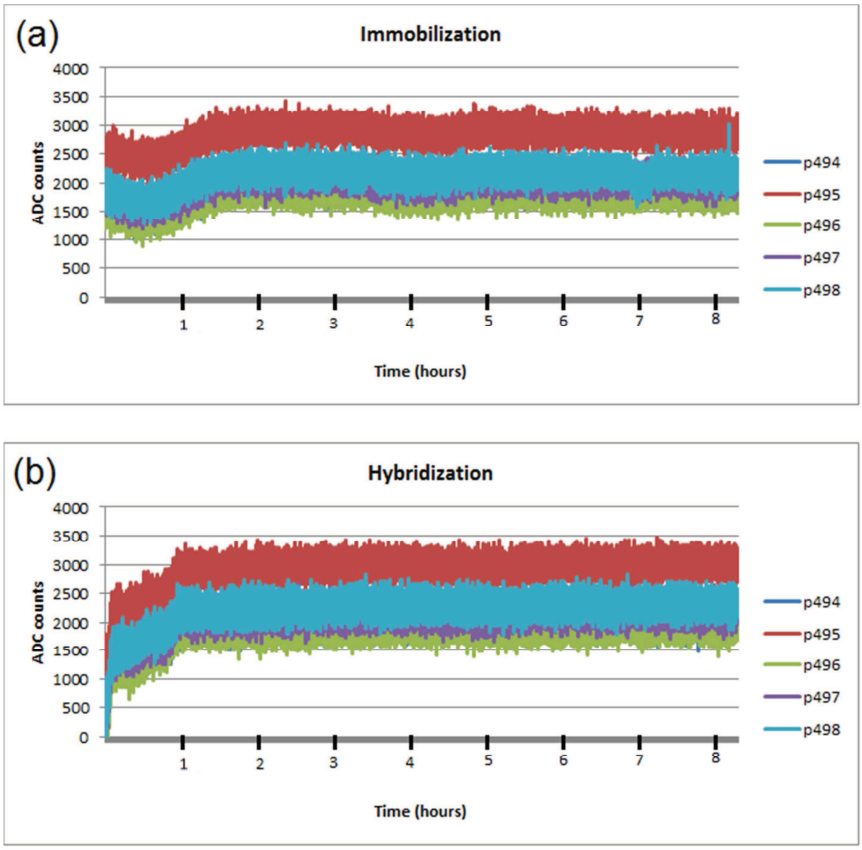

Figure 2.4: Leakage values of some pixels in immobilization and hybridization case. (a) Immobilization leakage result for 5 pixels (b) Hybridization leakage result in a 1pM, 30µL target DNA solution [9].

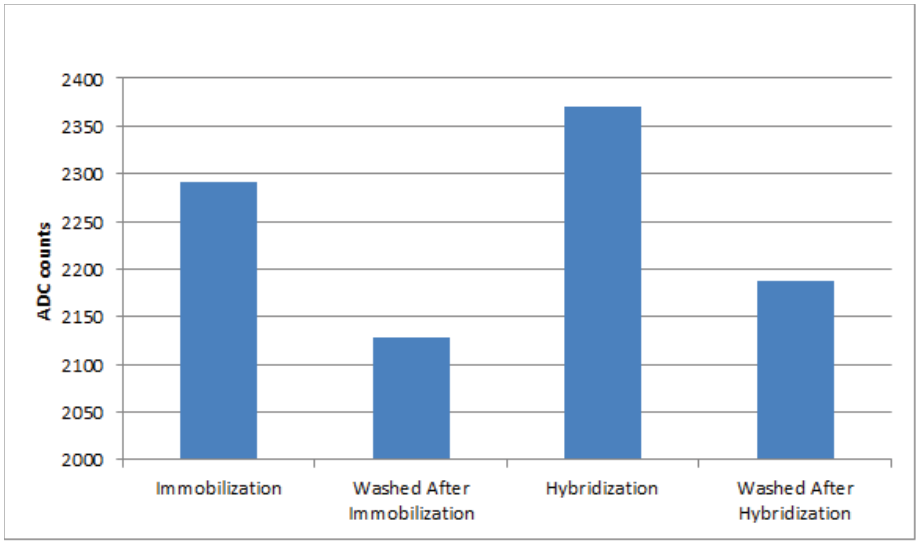

Figure 2.5: Average leakage of pixels in performed tests [9].

2.2 Modified CMOS Image Sensor for Cell Detection Tests

Figure 2.6 shows the pixel structure of the cell detection sensor. Cell detection tests in the scope of this thesis are performed with some modification made on the sensor used in DNA detection. The modification is done in the pixel structure. The top metal placed in the above sensor is eliminated, and the diffusion area of the source node of the reset transistor is enlarged.

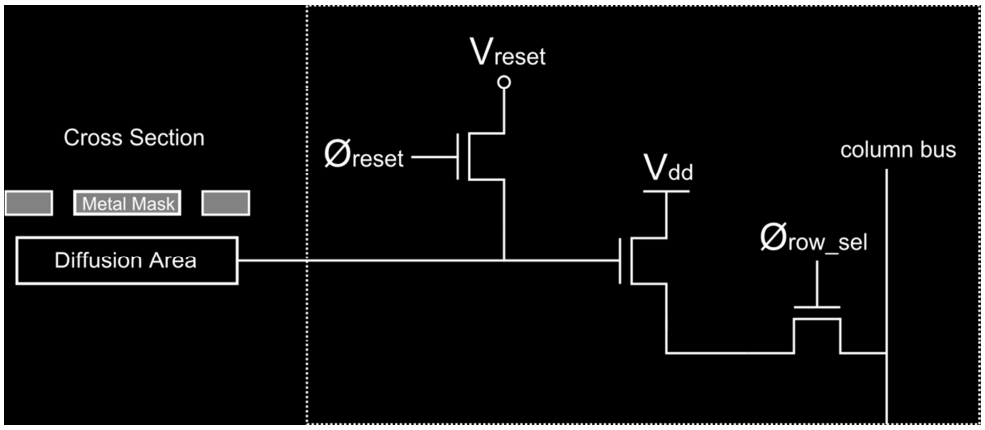

Figure 2.6: Pixel structure of the cell detection sensor.

Figure 2.7 shows (a) top view, (b) cross-section illustration, and (c) cell detection application of the pixel. The working principle of the sensor is totally changed compared to the DNA detection sensor. In the DNA detection sensor, capacitive sensing is performed while in this structure optical sensing is carried out. The sense node senses the incoming light according to the cells that are bound to the sensor array area. In Figure 2.7.(a), the whole surface except for four openings is covered with top metal as a light mask. However, metal layer in the middle of the four openings has no passivation layer on it for the surface activation for specific cell binding as seen in Figure 2.7.(b). Figure 2.7.(c) shows the diffusion areas that are open for the exposed light, can sense the light that reaches to those areas so the detection occurs in that manner.

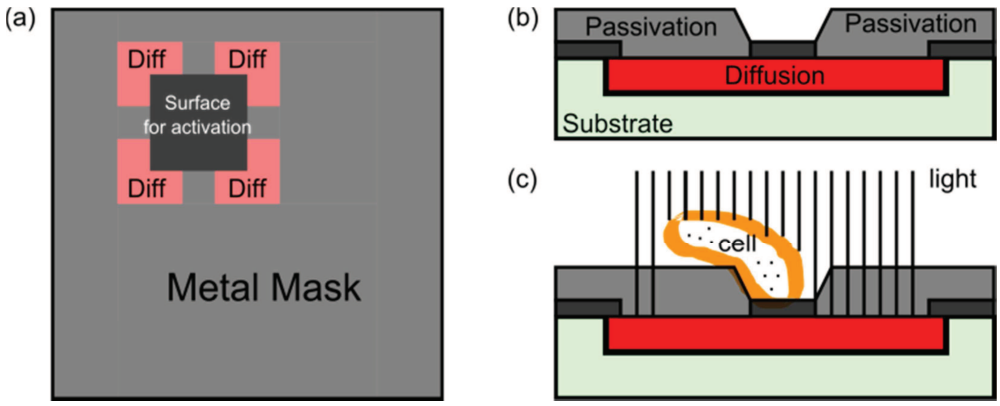

Figure 2.7: (a) Top view illustration of the pixel. (b) Cross-section illustration of the pixel. (c) Cell detection application of the pixel.

Figure 2.8 shows cross section view and top view photographs of the sensor package. Light is given to the sensor via leds that are fixed around the sensor, buried to the white epoxy. With this way, it is guaranteed that for every test, the amount of light that is exposed to the sensor is same. For this purpose, leds are biased with same voltage in order to get the same photon amount. Figure 2.8 illustrates, there is no additional layer between the sensor and the sample. Thus, the sample distance to the sensor surface is zero.

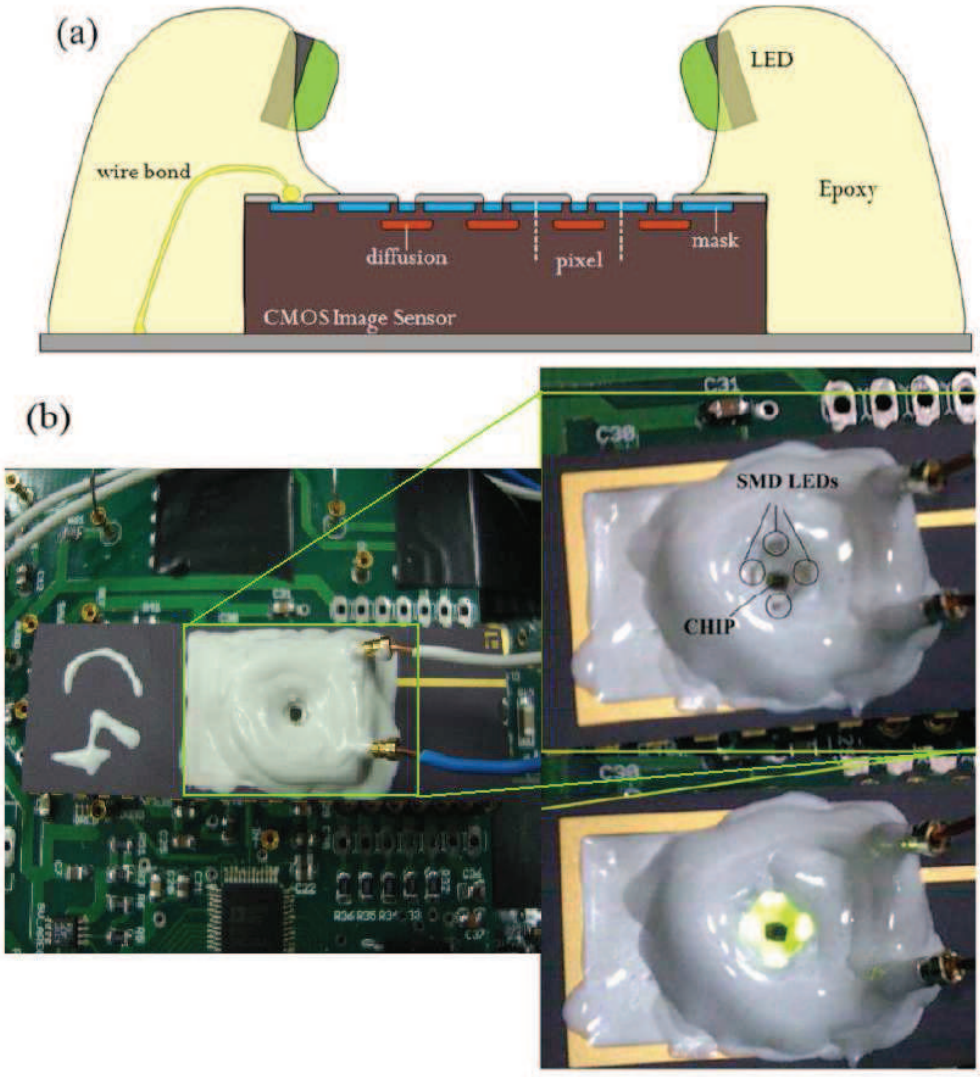

Figure 2.8: (a) Cross-section view of the sensor package, (b) Top view photograph of the sensor package.

2.2.1 Electroless Gold Coating over Aluminum Surface

Figure 2.9 shows the process steps of the electroless gold plating. The sensor surface is intended to be coated with gold in order to link the antibodies to the sensor surface. The coating is performed electroless in order not to prepare any mask that is suitable for the sensor. This will be hard because the sensor samples are in the die level, and electroplating will be harder in die level process.

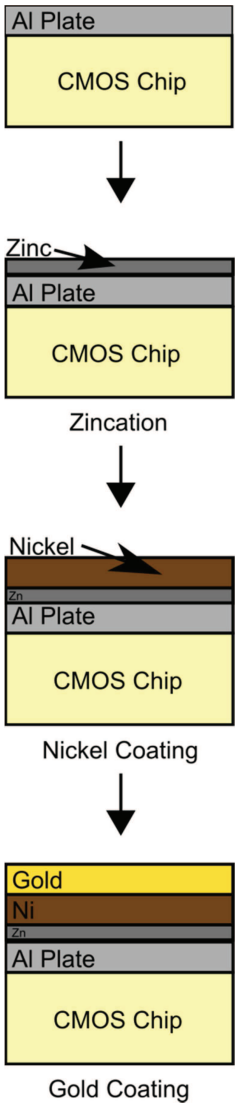

Figure 2.9: Process steps of electroless gold plating.

The top metal of the standard CMOS process, aluminum, should be coated with gold in order to immobilize the antibodies. For this purpose, first, the aluminum surface is subjected to zincation process. This step is a preparation step for nickel coating. After zincation, electroless nickel coating is done, and finally gold is coated over nickel. Figure 2.10 to Figure 2.13 show the scanning electron microscope (SEM) pictures and EDS results of the aluminum metal surface and the electroless gold coated surface.

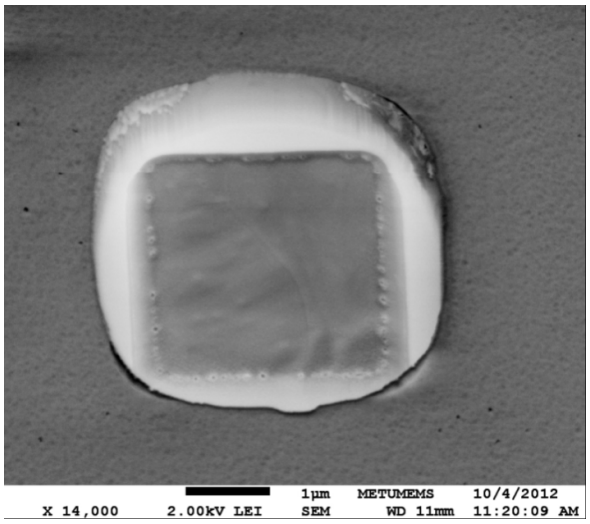

Figure 2.10: SEM picture of single Al pixel. Pixel size is 3µm × 3µm.

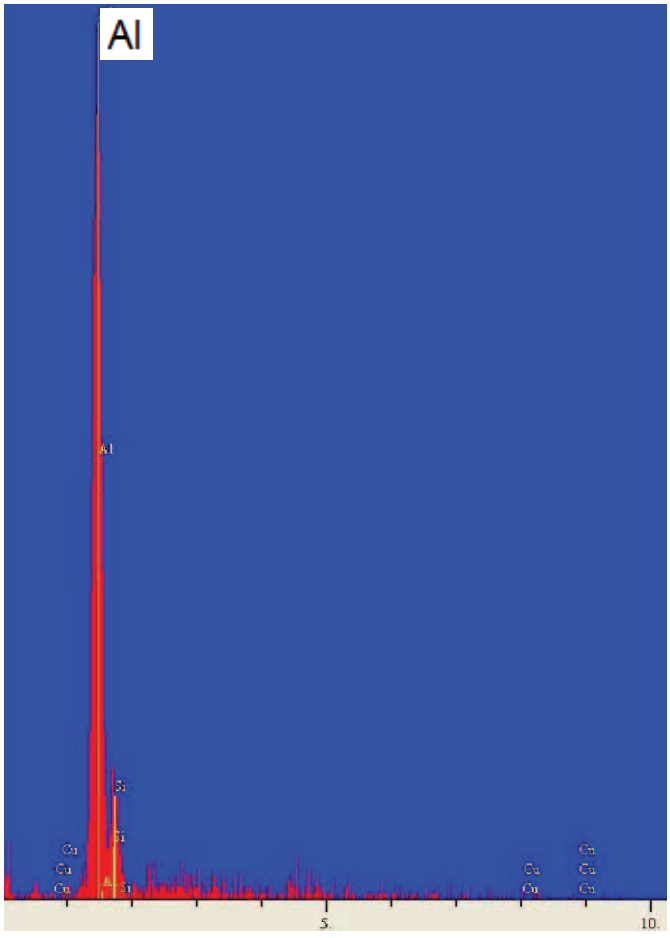

Figure 2.11: EDS result of single Al pixel.

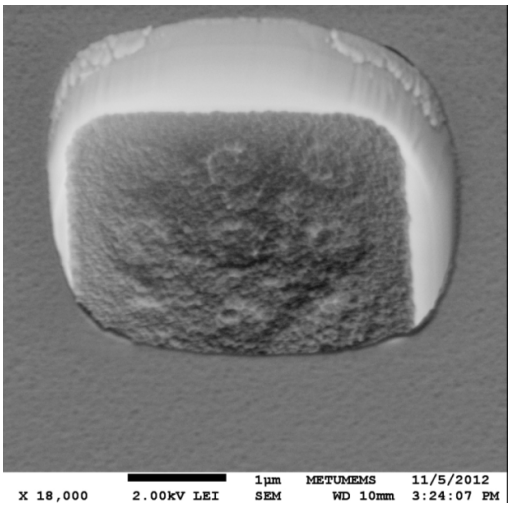

Figure 2.12: SEM picture of single gold coated pixel.

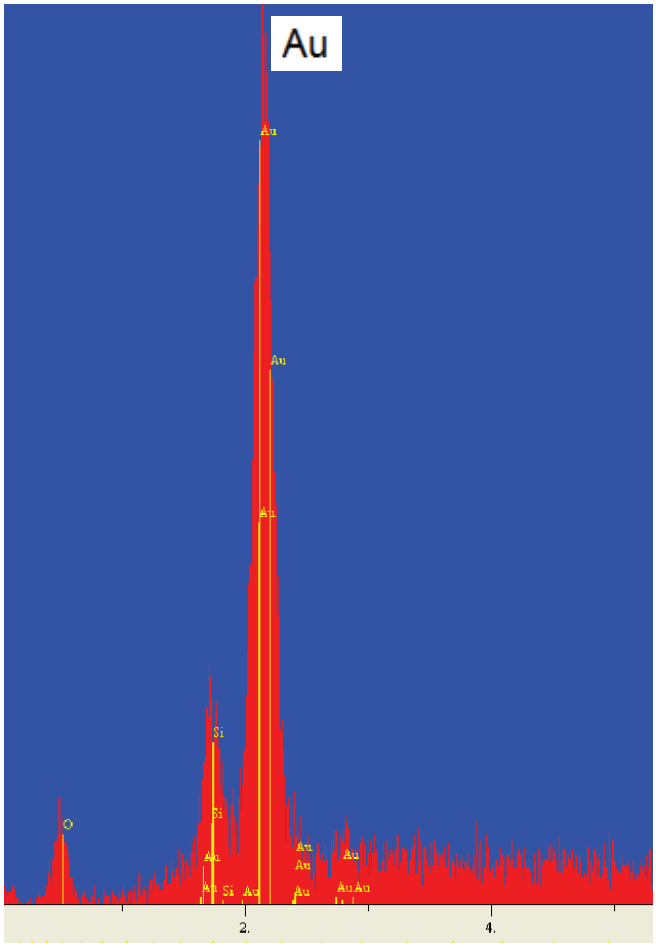

Figure 2.13: EDS result of single gold pixel.

2.3 Cell Detection Test Results

Cell tests performed in the scope of this thesis can be divided into two parts: (i) first tests are carried out with baker's yeast cells (*Saccharomyces cerevisiae*) and (ii) second tests are carried out with MCF-7 breast cancer cells.

To show the cell detection capability of the sensor with the proposed method (shadowing method), first tests are done with yeast cells. As mentioned in the introduction chapter, cells that will be detected have to be placed zero distance away from the sensor surface. For this purpose, yeast cells are chosen for detection because of their cell walls around their core cell. The PBS solution is dried to transfer the yeast cells to the sensor surface. When the yeast cell containing solution is dried, the cells will be transferred to the sensor surface with zero distance. The important point here is that when the solution dries, the cells must not die to detect them so the cell wall that encircles them avoids killing the cells. The solution that will be used for the tests is chosen as phosphate buffered saline (PBS) because after this yeast cell tests, breast cancer cell tests will be performed, and in these tests, PBS solution is required for the cells to be remain alive.

Figure 2.14 shows clustered yeast cells that are transferred directly from PBS solution. Previous tests show that yeast cells that are transferred directly from PBS solution form clusters that do not give possibility to detect single cells.

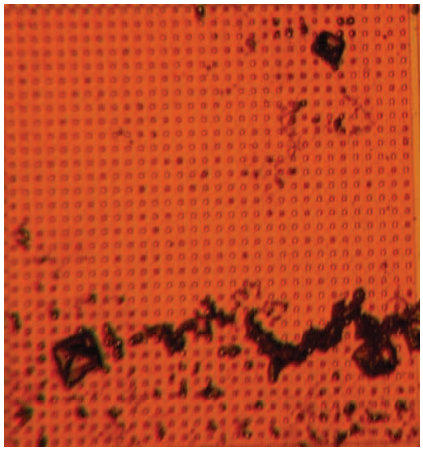

Figure 2.14: Clustered yeast cells that are transferred directly from PBS solution.

After getting this result, yeast cells are waited in glucose concentrated DI water to grow and separate from each other. The grown yeast cells are than put into PBS solution for testing. Figure 2.15 shows (a) microscope photograph of dried yeast cells that are grown in glucose concentrated DI water and (b) related sensor image.

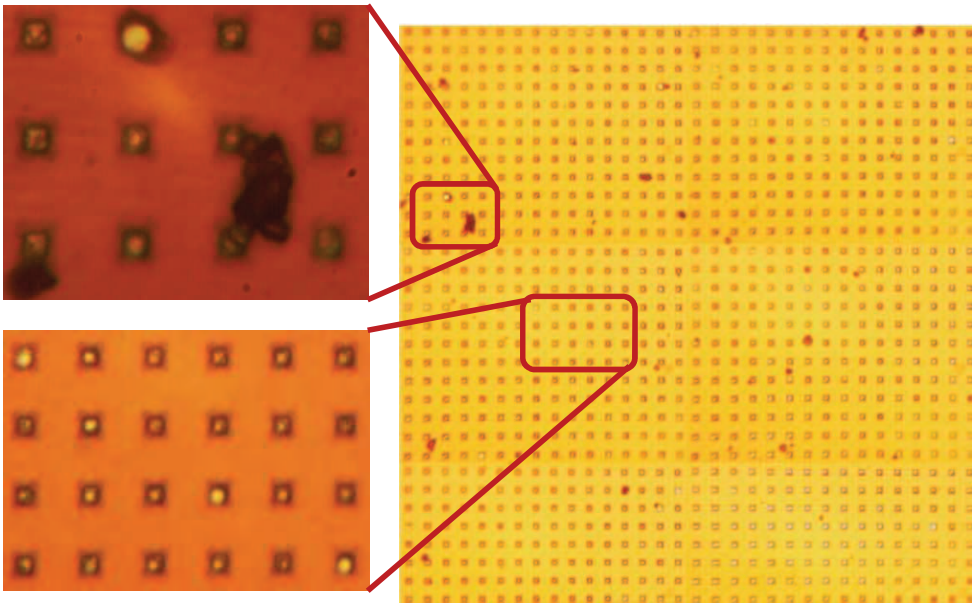

(a)

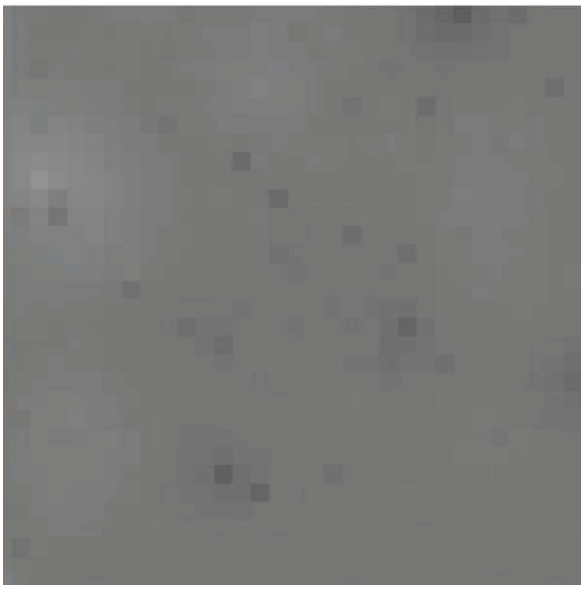

(b)

Figure 2.15: (a) Microscope photograph of dried yeast cells that are grown in glucose concentrated DI water, and transferred to PBS solution, (b) Related sensor image.

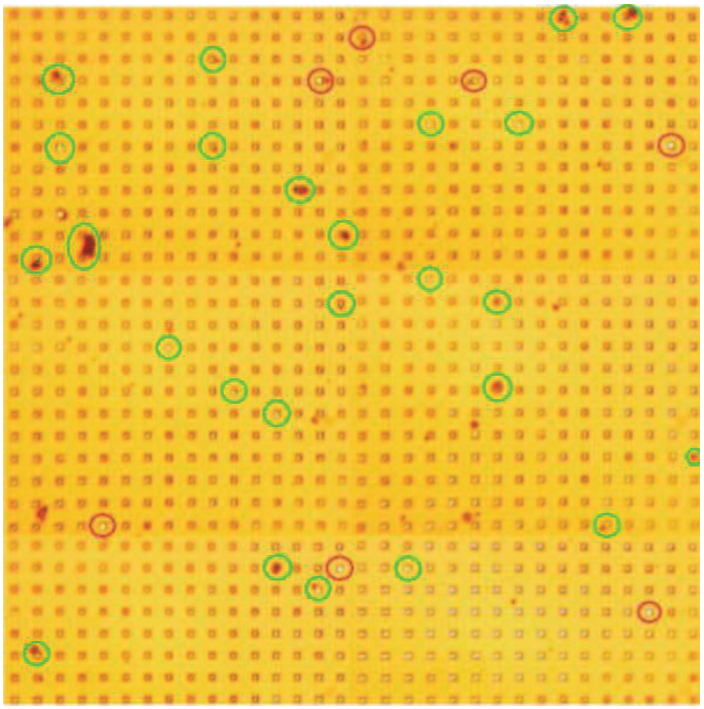

(a)

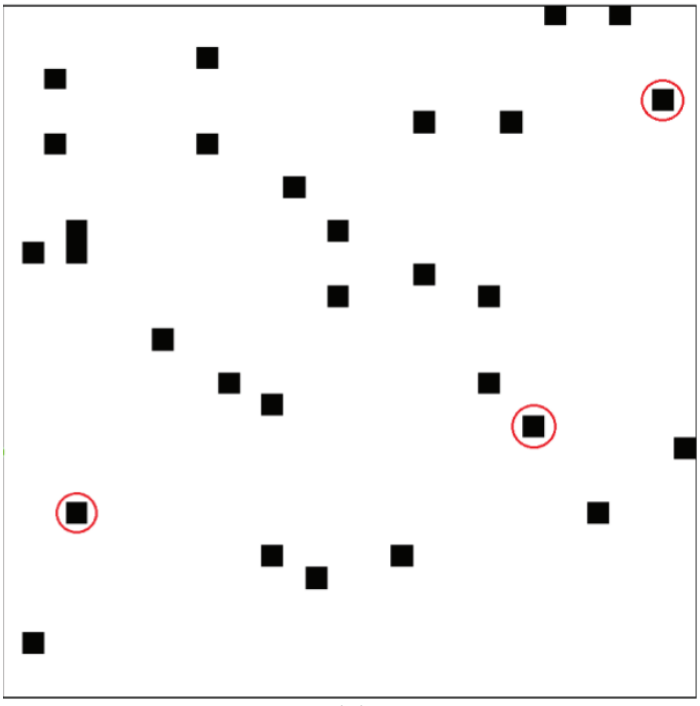

(b)

Figure 2.16: (a) Microscope photograph of the sensor. Red circles show the cells that cannot be detected, and green circles show the cells that are detected. (b) Image processed sensor image. Red circles show pixels that have no cells on it.

Figure 2.16.(a) shows microscope photograph of the sensor. Red circles show the cells that cannot be detected, and green circles show the cells that are detected. Figure 2.16.(b) shows image processed sensor image. Red circles show pixels that have no cells on it. After taking the sensor image, some processing is applied. A threshold is determined between the pixels, and the pixels above the threshold is shown as black and the rest is shown as white. As a result, image sensor detects 72% of the yeast cells that are placed in the sensor array. The reason of the missed cells can be grouped into two reasons. One reason is that the certain smaller yeast cells are just placed in the 3µm × 3µm pit and cannot cancel the coming light to the sensing area. Second reason can be the cells that are placed near the sensing areas cannot significantly prevent the coming light to the sensing area and thus, sufficient contrast could not be obtained.

After taking these results with yeast cells, breast cancer cell (MCF-7) tests are performed. Figure 2.17 shows the structures of yeast cell wall and MCF-7 cell membrane. The most significant difference between yeast cells and MCF-7 cells are the structures that cover them. Yeast cells have cell walls around that protect them from bursting because of desiccation of the medium while MCF-7 cells have only cell membranes that are not strong enough to maintain them as a whole.

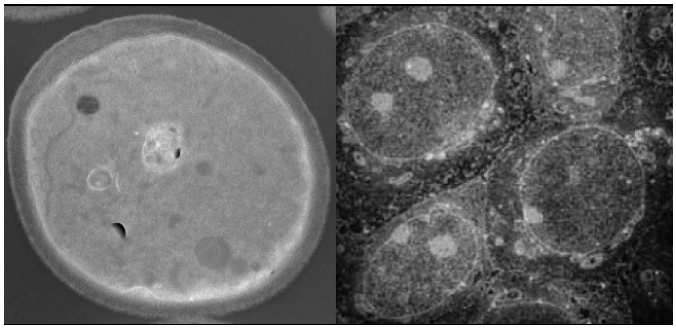

(a) (b)

Figure 2.17: Structures of (a) yeast cell wall and (b) MCF-7 cell membrane

Because of the cell membrane structure of MCF-7 cells like all other cancer cells, the medium of these cells cannot be desiccated. Without their medium, they cannot survive.

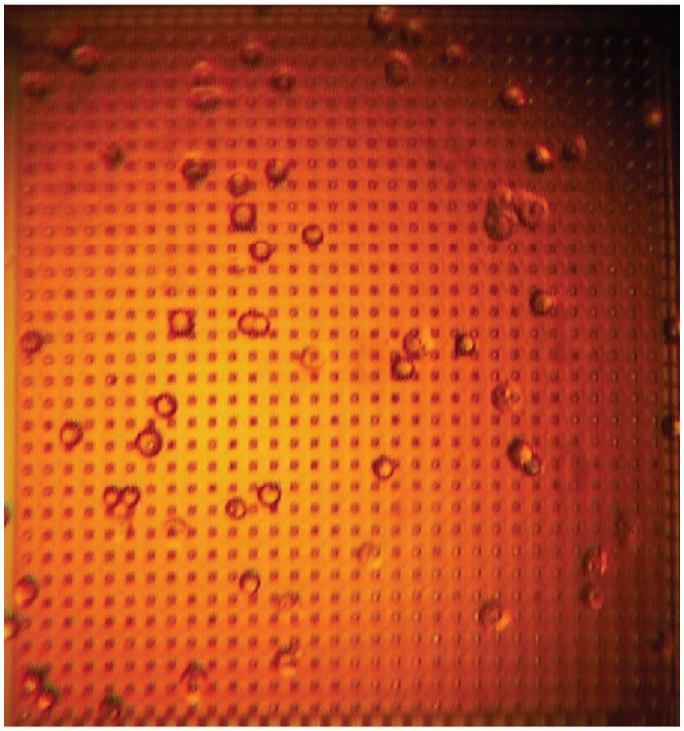

(a)

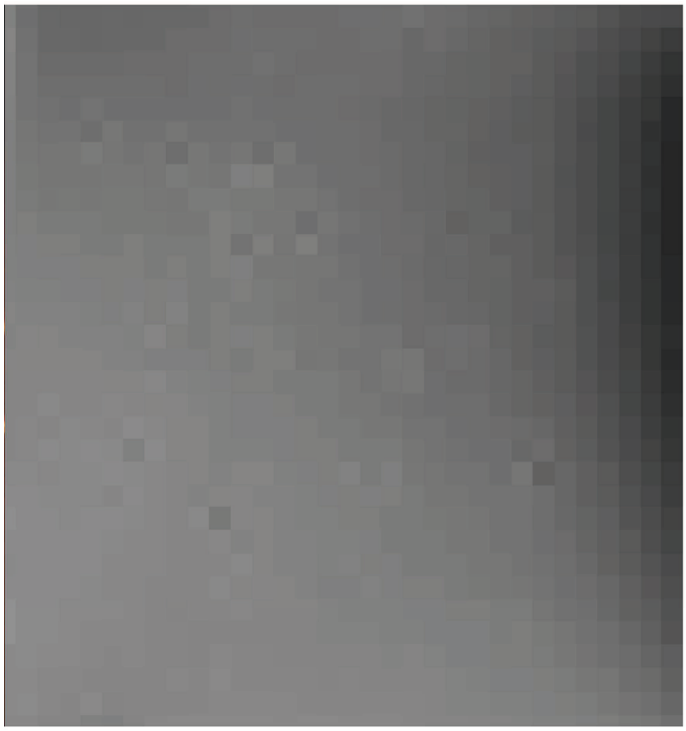

(b)

Figure 2.18: (a) Microscope photograph of MCF-7 cells in PBS solution, (b) Related sensor image.

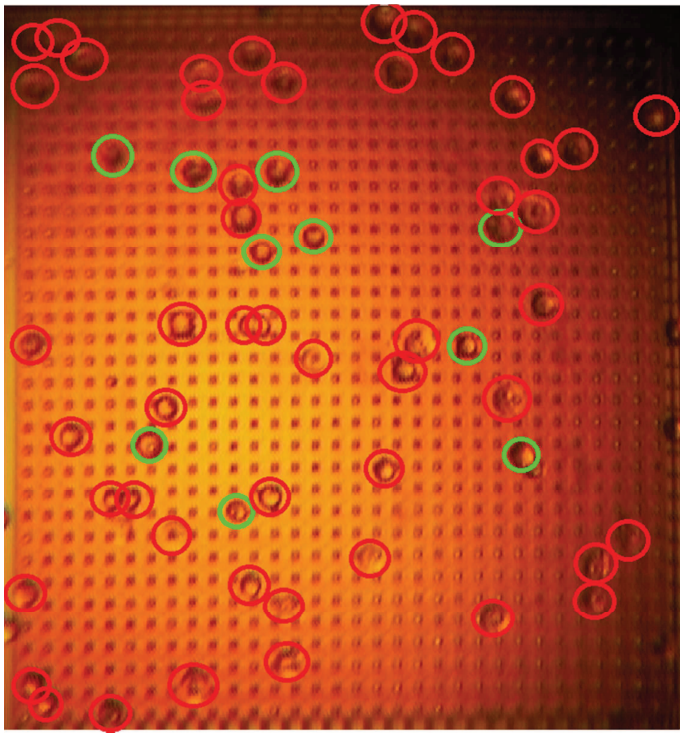

(a)

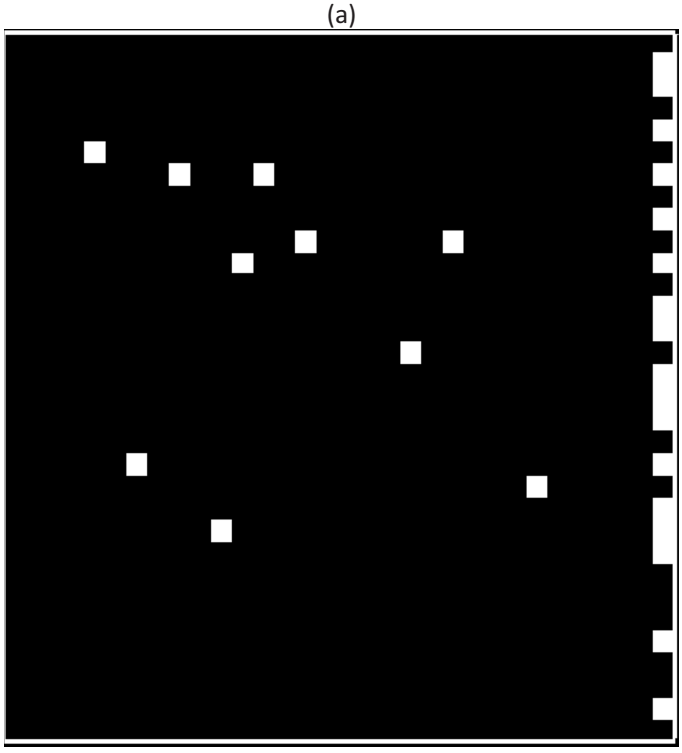

(b)

Figure 2.19: (a) Microscope photograph of the sensor. Red circles show the cells that cannot be detected, and green circles show the cells that are detected. (b) Image processed sensor image.

Figure 2.18 shows the microscope photograph and related sensor image of MCF-7 cells in PBS solution. It can be seen that most of the cells cannot be detected because of the fact that photons in the liquid medium spreads arbitrarily, and the shadows of the cells cannot be formed sufficiently. Figure 2.19.(b) shows the image processed sensor image. Only 10 cells out of 59 cells can be detected in the medium when the medium is not desiccated.

The only way that the sensor image to be taken is to take the sensor image when the medium is about to dry in order to place the cells above zero distance from the sensor surface. There is some time while the medium is drying for cells not to be died. Figure 2.20 shows (a) microscope photograph of MCF-7 cells in PBS solution while the solution is about to dry and (b) related sensor image. The successful images can be taken only the cells are placed zero distance from the sensor surface. Figure 2.20.a shows that the focusing effect can be observed from the left bottom of the sensor. A cell out of the sensor array focused the exposed light to the inside of the sensor area.

Again, the image is processes in the same way with the above example. Figure 2.21 shows the resulting image. Results show 63 cells are detected among 68 cells with this technique. Sizes of the MCF-7 cells are different from each other so some cells affect only one pixel and some are more than one pixel, thus it cannot be said that every white pixel in the sensor image corresponds to a single cell or if a percentage is has to be given; if one pixel corresponds to a single cell, the success rate of the sensor is 78%. The reason why the pixel colors of detected cells are brighter is focusing effect. As explained in Section 1.1, cells show focusing effect to the sensor surface meaning that they focus the incoming light to the sensor area making the pixels brighter.

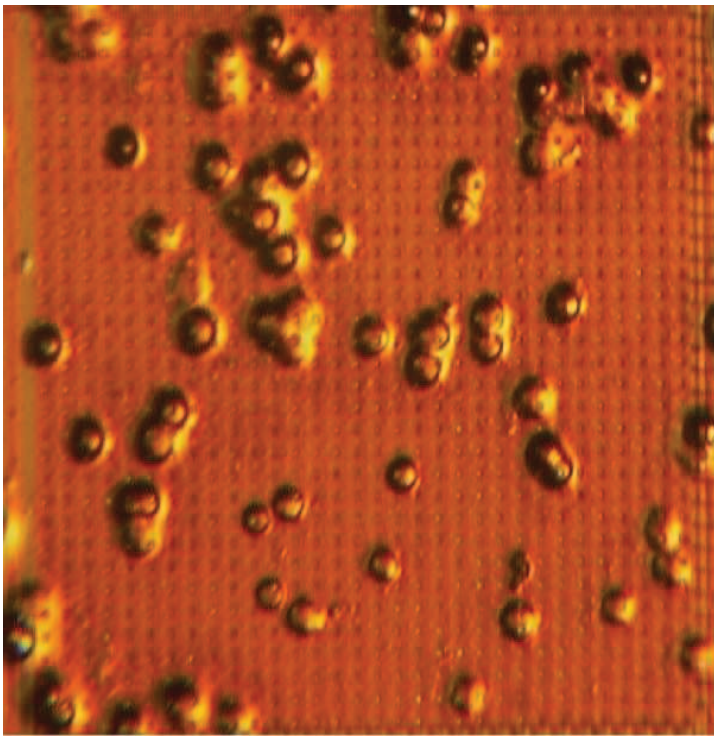

(a)

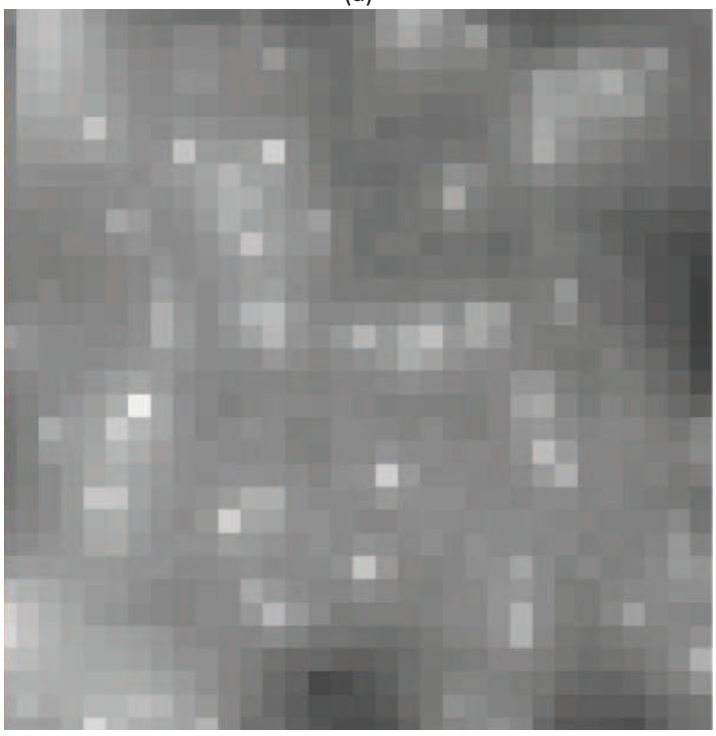

(b)

Figure 2.20: (a) Microscope photograph of MCF-7 cells in PBS solution while the solution is about to dry, (b) Related sensor image.

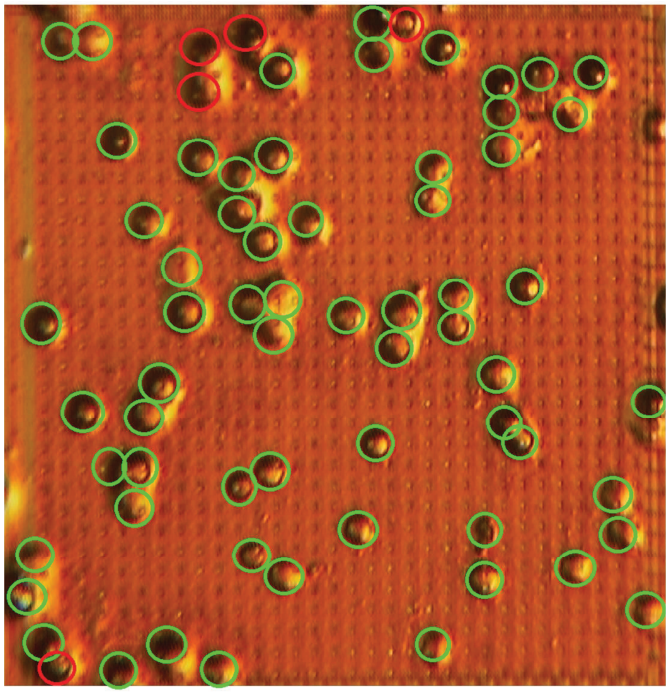

(a)

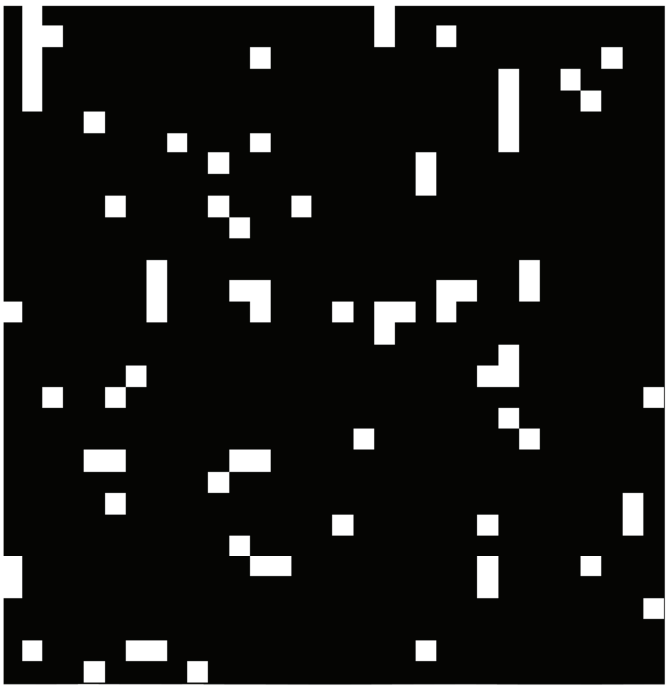

(b)

Figure 2.21: (a) Microscope photograph of the sensor. Red circles show the cells that cannot be detected, and green circles show the cells that are detected. (b) Image processed sensor image.

Figure 2.22 and Figure 2.23 show microscope photographs and sensor images of dead MCF-7 cells when the solution is fully dried. It cannot be discussed about the detection rate of the cells because most cells are burst and cannot be visualized as can be seen from the figures.

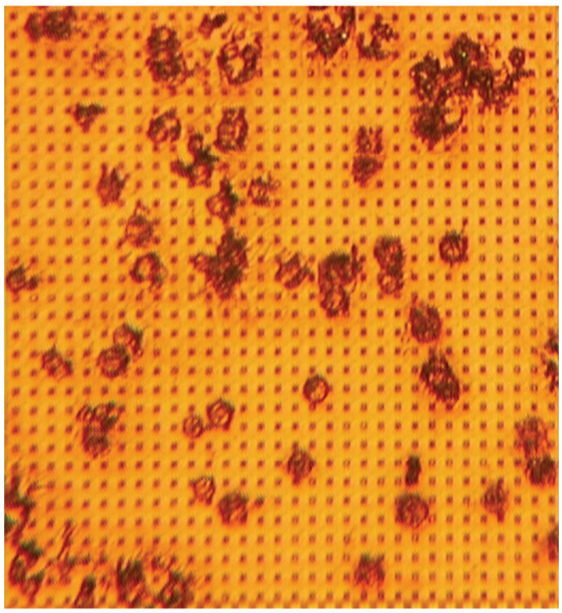

(a)

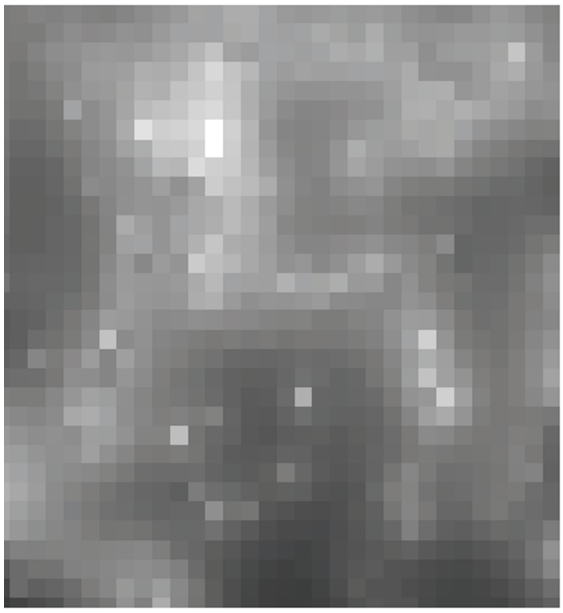

(b)

Figure 2.22: (a) Microscope photograph of dead MCF-7 cells when the solution is fully dried, (b) Related sensor image.

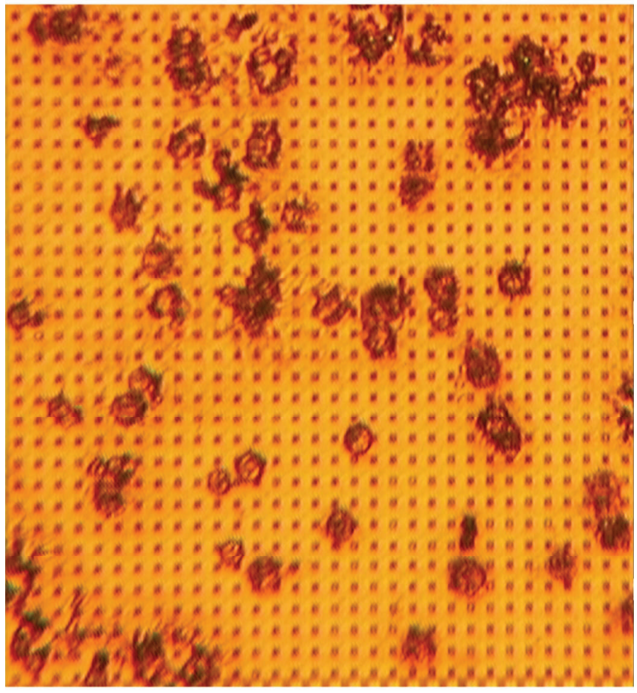

(a)

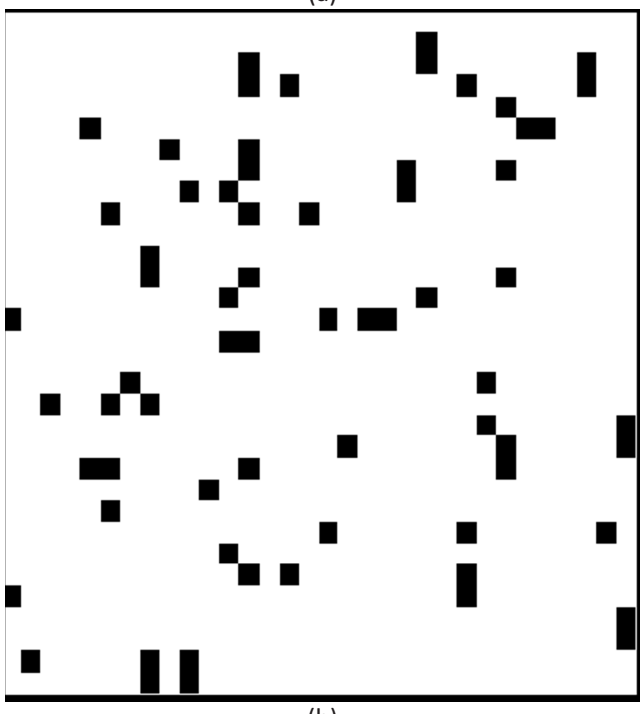

(b)

Figure 2.23: (a) Microscope photograph of dead MCF-7 cells when the solution is fully dried. (b) Image processed sensor image.

After taking this successful result, it is thought that if these cells are bound to sensor surface anyhow, while the cells are in their living medium (PBS), maybe the sensor image can be taken. For this purpose, drug resistant MCF-7 cells are used for specifically binding to antibodies. The only difference between basic MCF-7 cells and drug resistant MCF-7 cells is the P-glycoprotein that exists on their outer surfaces [26]. If this P-glycoprotein can be bound to its antibody, anti-P-glycoprotein, maybe cells that are bound to the surface can be detected. Another advantage of the antibody is to detect the desired cell. If the antibody of any desired cell can be linked to the sensor surface, these cells will be bound to surface, and any other cells that are not sensitive to this antibody will be washed out with washing the sensor. In order to realize this proposal, the sensor surface has to be coated with gold. Gold is necessary for the antibodies to bind. In Section 2.2.1, gold coating of the activation surfaces has been explained in detail.

The next process after coating the activation surfaces with gold is immobilizing these gold surfaces with anti-P-glycoprotein antibodies. Figure 2.24 antibody binding process to the gold coated surfaces. First of all, 12µL anti-P-glycoprotein is mixed with 20mM, 3µL sulfo-LC-SPDP linkers and then waited for 90minutes. After 90minutes, 7µL TCEP-HCl is added to the solution, and this mixture is added to the sensor surface and waited 60minutes more. In this 60minutes, TCEP-HCl molecules break down the di-sulfide links obtaining the immobilization of antibodies over gold surfaces. After waiting 60minutes, the sensor surface is washed and sensor is ready for adding MCF-7 cells for binding to their antibodies.

Figure 2.25 shows MCF-7 cell washing process when they are bound to the antibodies. After immobilizing antibodies on the gold surfaces of the sensor, MCF-7 cells are placed and exposed to them. Then, cells are waited 60minutes on the sensor surface. After waiting 60minutes, sensor is washed with PBS. Figure 2.25.(b) shows the microscope photograph of the sensor. In Figure 2.25.(a), the cells that are washed out are circled in yellow. One more washing process is done, and the result is shown in Figure 2.25.(c). In Figure 2.25.(b), the cells that are washed out are circled in yellow. Third washing

process is again done, and this time no other cells are washed out. Figure 2.25.(d) shows the cells that are bound strongly to the antibodies.

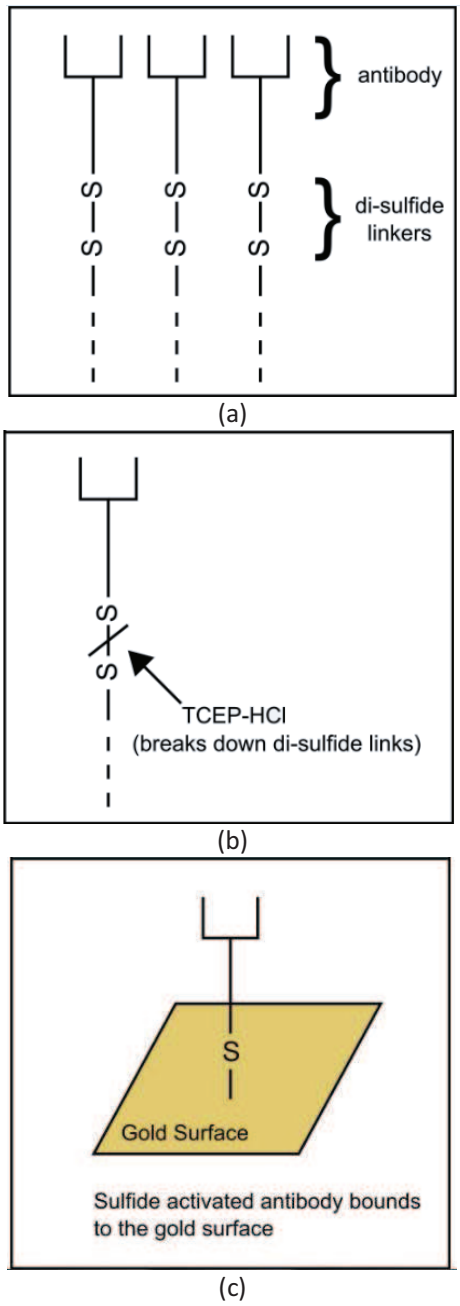

Figure 2.24: Antibody binding process to the gold coated surfaces (a) First step is mixing antibodies with linkers which will be soon link the antibody to the gold surface. (b) Adding TCEP-HCl for breaking down di-sulfide links. (c) Adding this solution to the sensor surface for immobilizing the antibodies.

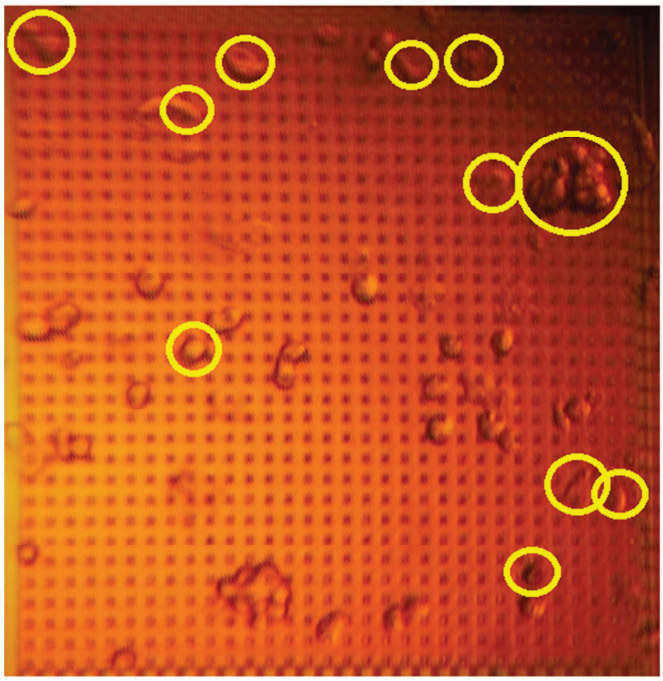

(a)

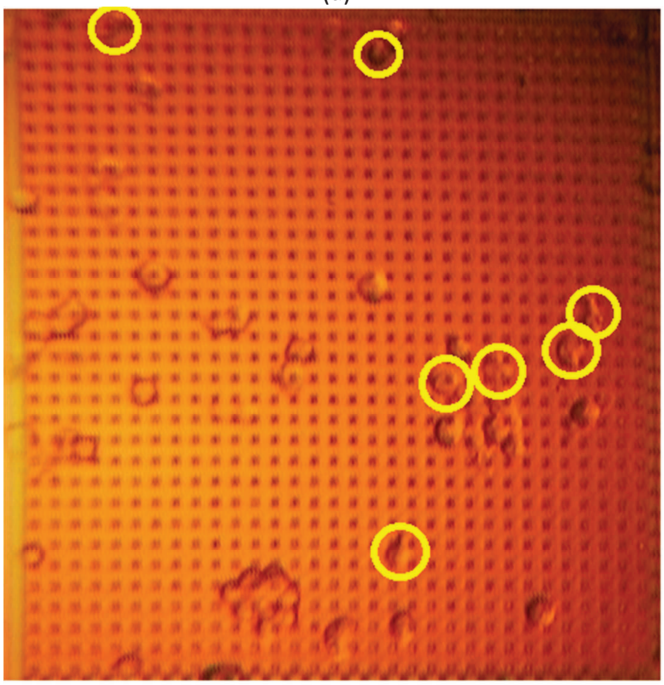

(b)

Figure 2.25: MCF-7 cell washing process when they are bound to the antibodies. (a) Microscope image of the MCF-7 cells that are placed on the antibody immobilized sensor one hour (Yellow circled cells are that of washed out). (b) Microscope image of the MCF-7 cells after first washing (Yellow circled cells are that of washed out). (c) Microscope image of the MCF-7 cells after second washing. (d) Microscope image of the MCF-7 cells after third washing.

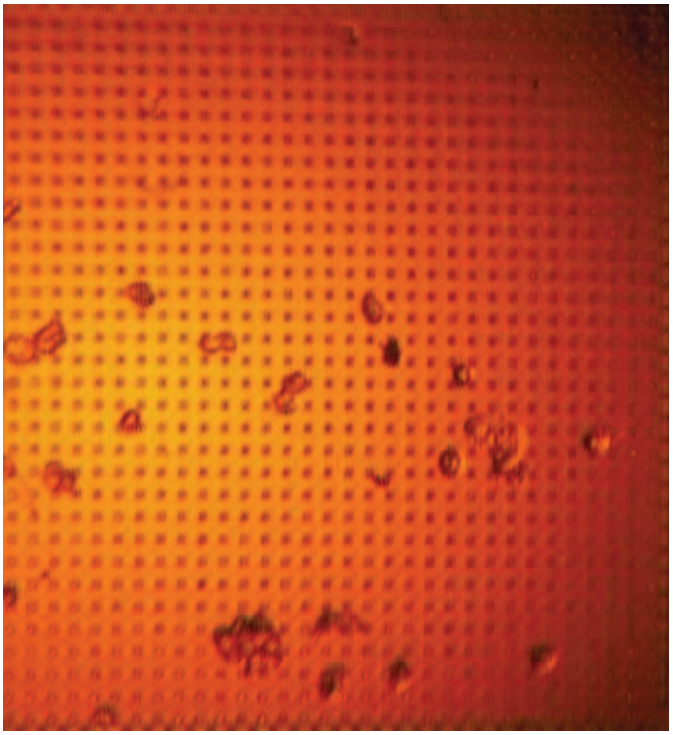

(c)

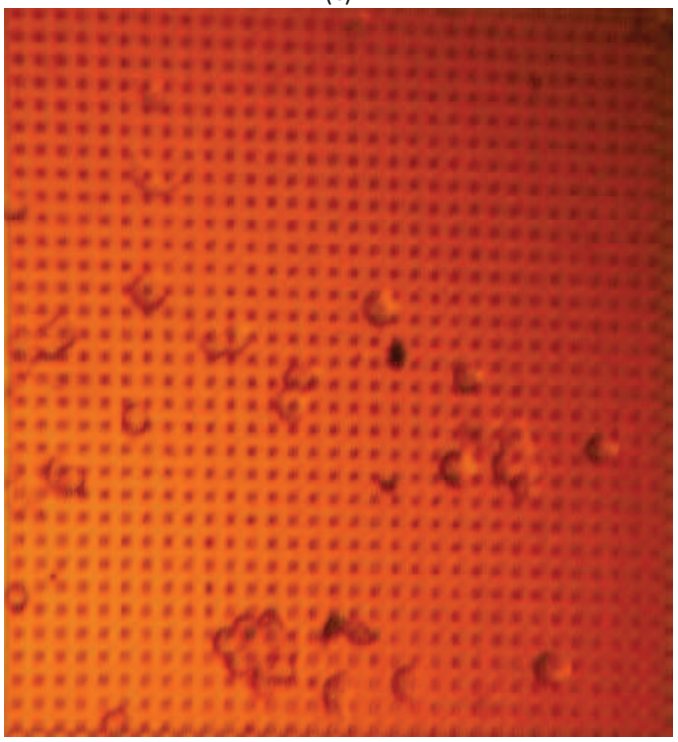

(d)

Figure 2-25: cont'd

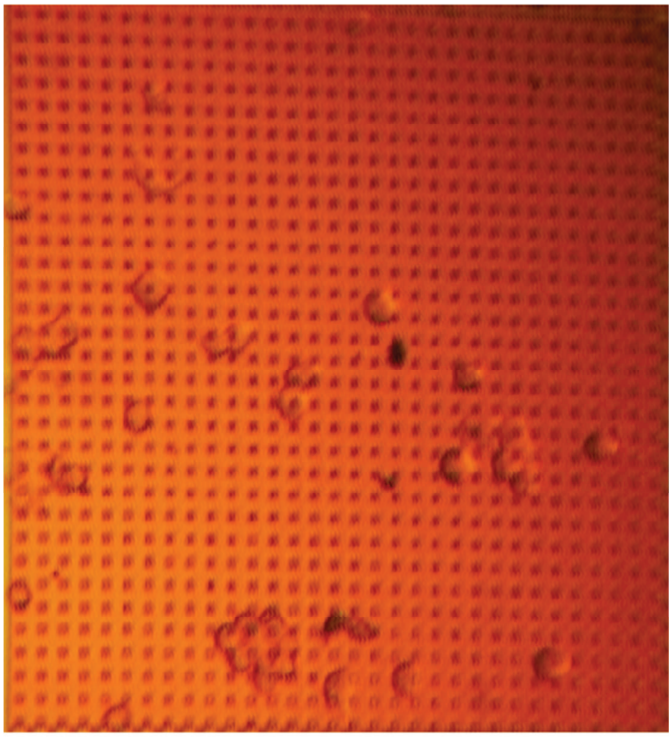

(a)

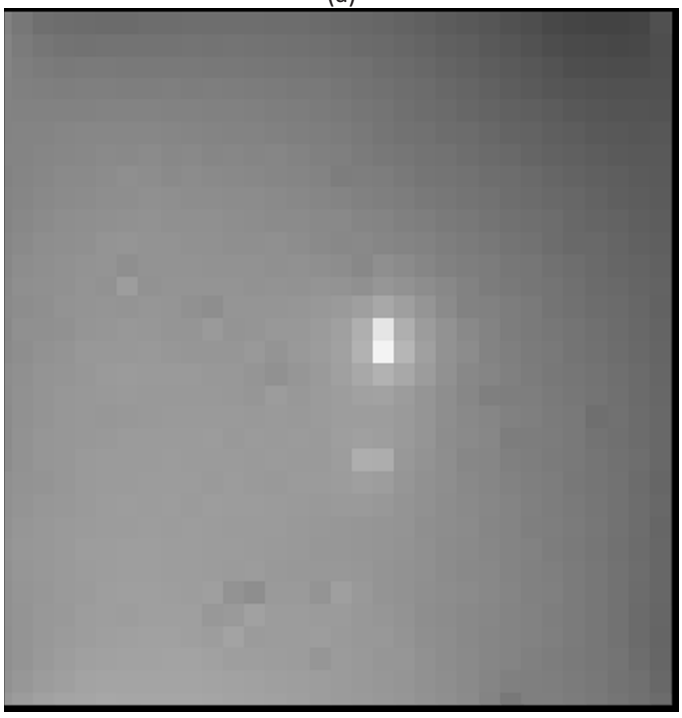

(b)

Figure 2.26: (a) Microscope photograph of MCF-7 cells that are bound to antibody, and remains on the sensor surface after three washing, in PBS solution, (b) Related sensor image.

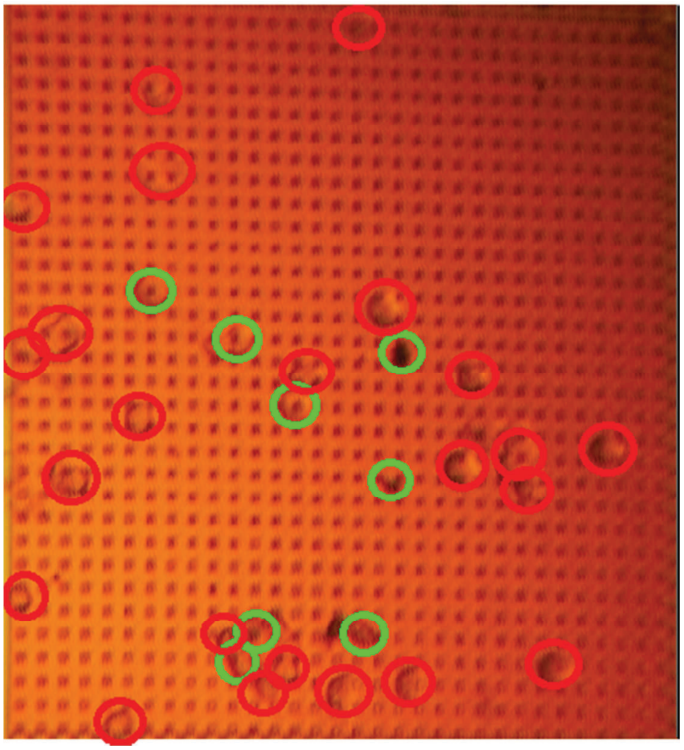

(a)

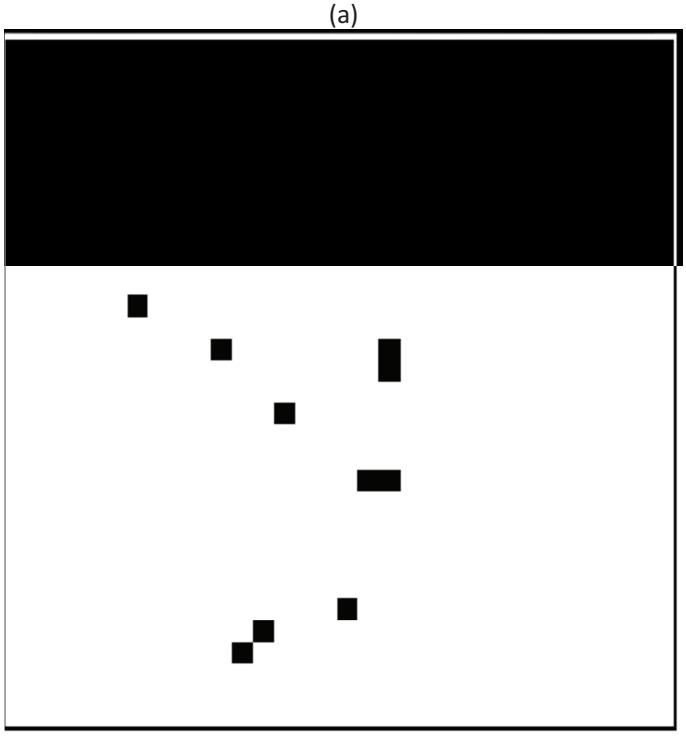

(b)

Figure 2.27: (a) Microscope photograph of the sensor. Red circles show the cells that cannot be detected, and green circles show the cells that are detected. (b) Image processed sensor image.

Figure 2.26 shows the microscope photograph of MCF-7 cells that are bound to antibody, and remains on the sensor surface after three washing, in PBS solution. Again in PBS solution, sensor image does not give sufficient information. Figure 2.27.(b) shows the image processed sensor image. This results show that the only reason why the sensor cannot get successful images in PBS solution is that the solution spreads the incoming photons. Thus, shadows of the cells cannot be formed even if the cells are zero distance away from the sensor image.

Figure 2.28 and Figure 2.29 substantiates this statement that when the solution is about to dry, the sensor can get sufficient images. It should be noted that 74% of the cells are detected with the image sensor if the cluster is excluded. If included, 69% success is obtained.

Another result of this test is that the sensor can differentiate dead and live cells. Figure 2.30.(b) shows image processed sensor image of the dead cells. Dead cells prevent incoming photons to the sensor instead of focusing like live cells. The missed dead cell probably cannot be detected because it is placed in the middle of two detectors.

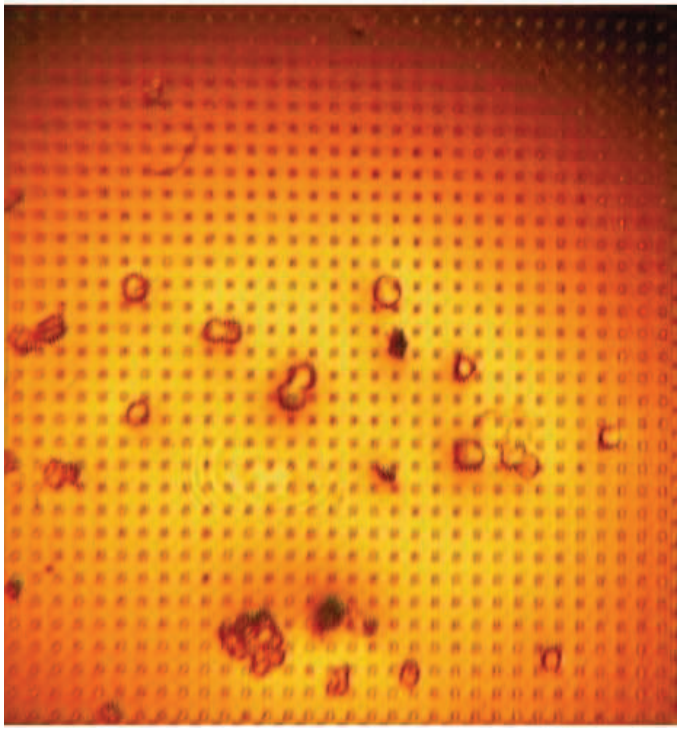

(a)

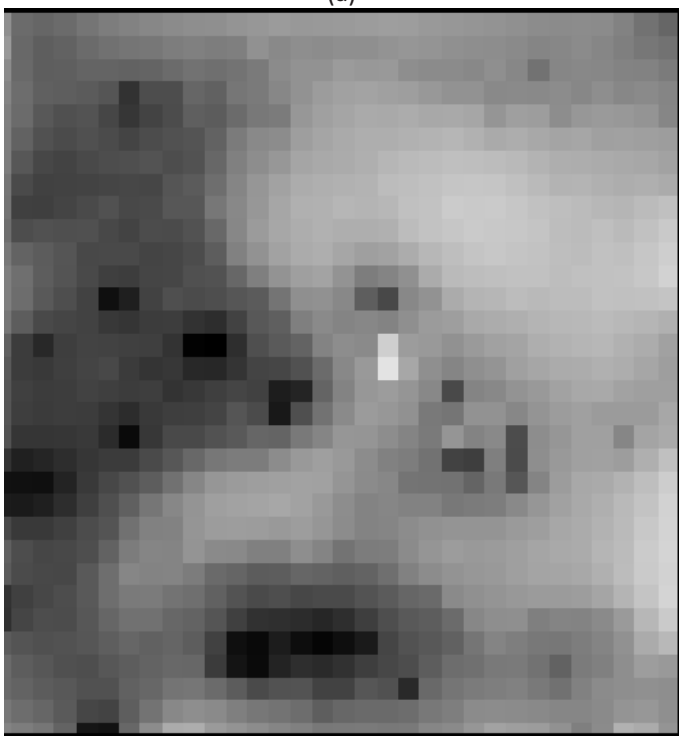

(b)

Figure 2.28: (a) Microscope photograph of MCF-7 cells that are bound to antibodies in PBS solution while the solution is about to dry, (b) Related sensor image.

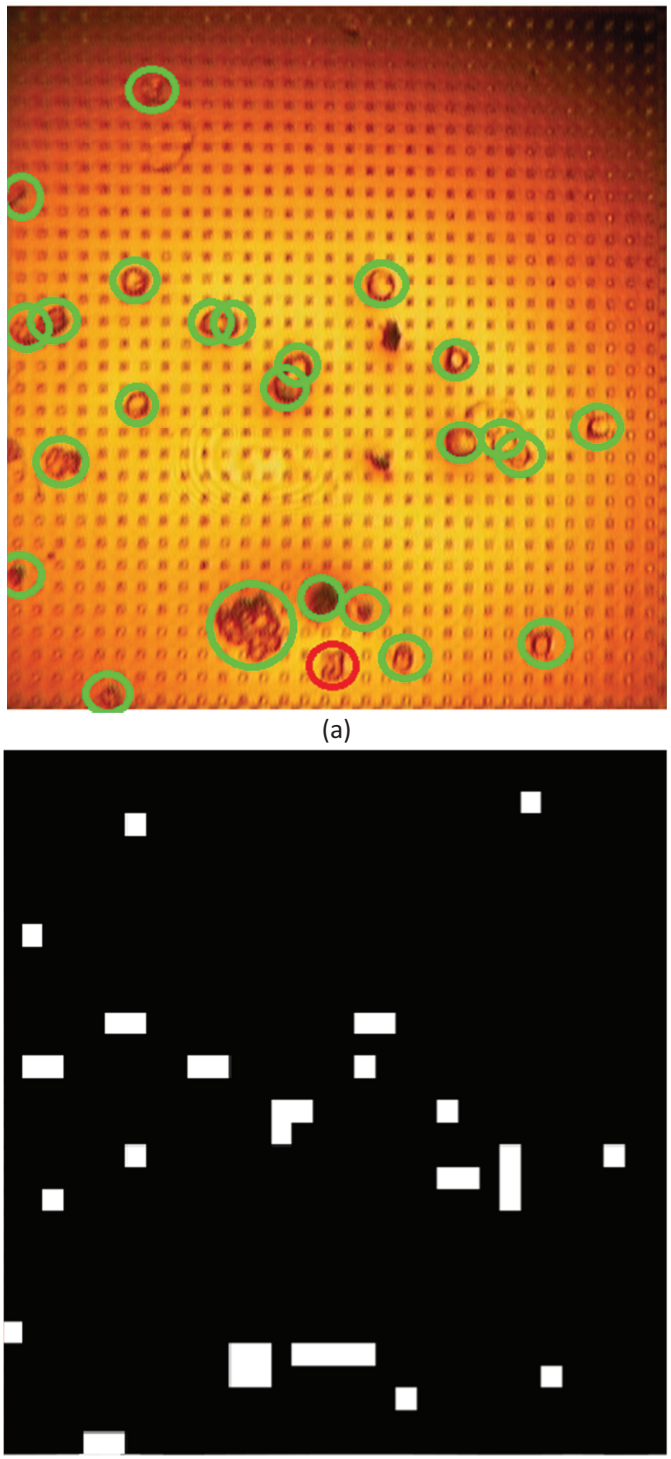

(a)

(b)

Figure 2.29: (a) Microscope photograph of the sensor. Red circles show the cells that cannot be detected, and green circles show the cells that are detected. (b) Image processed sensor image that shows live cells.

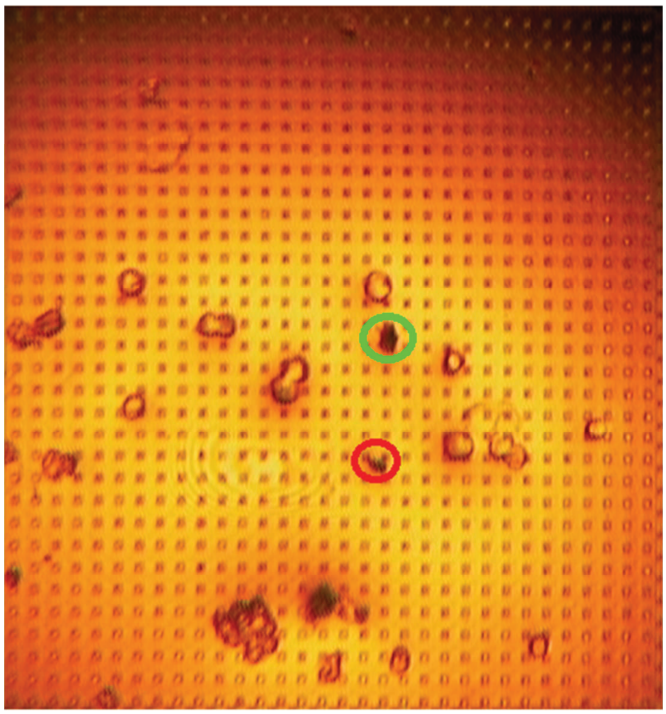

(a)

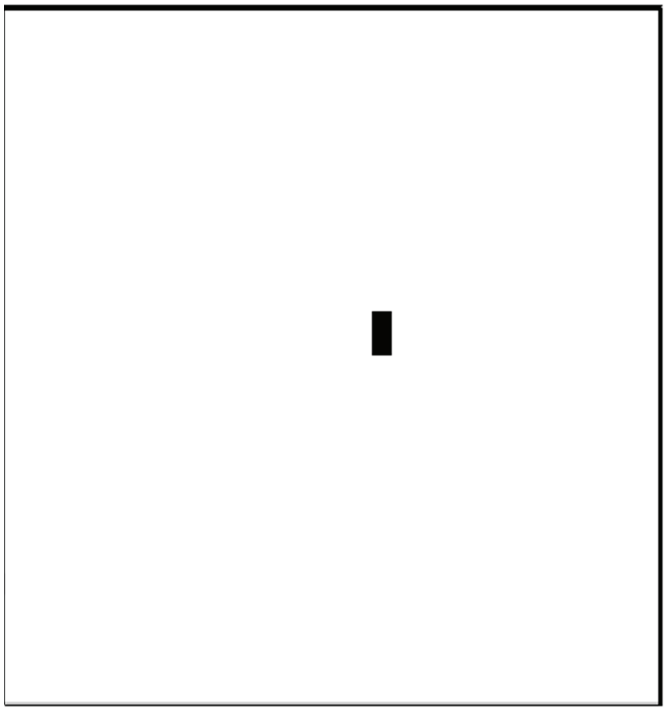

(b)

Figure 2.30: (a) Microscope photograph of the sensor. Red circles show the cells that cannot be detected, and green circles show the cells that are detected. (b) Image processed sensor image of the dead cells.

After taking these results, as a control test, a sensor without binding antibodies on its surface is tested. Figure 2.31 shows MCF-7 cell washing process with a sensor that has no antibodies on it. All of the cells are washed out after third washing, and it is guaranteed that in the previous tests, the MCF-7 cells are bound to the sensor surface because of the antibodies.

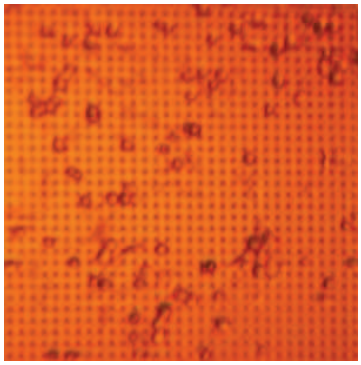

(a)

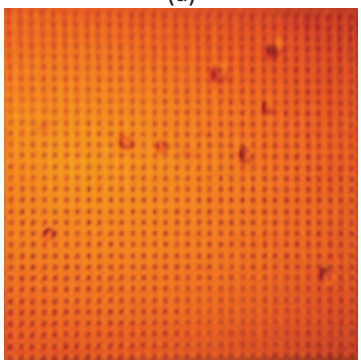

(b)

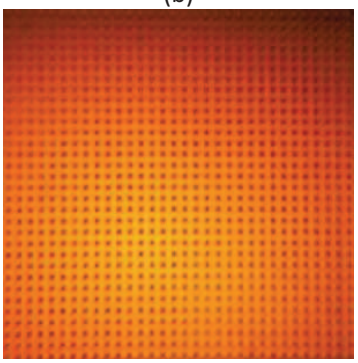

(c)

Figure 2.31: MCF-7 cell washing process with a sensor that has no antibodies on it. (a) Microscope image of the MCF-7 cells that are placed on the sensor without antibody binding one hour. (b) Microscope image of the MCF-7 cells after first washing. (c) Microscope image of the MCF-7 cells after second washing.

CHAPTER III

THE CELL DETECTION IMAGING SENSOR

According to the cell detection test results that have obtained from the image sensor, a more advanced CMOS image sensor is designed. This chapter explains all the building blocks of the new cell detection imaging sensor in detail. This chapter also gives how each of the designed block works, and what kinds of signals are required for the proper operation. Simulation results of each block will be presented comparing with the necessary proper values that is required for the proper operation.

This chapter is organized as: Section 3.1 gives a brief introduction about the imaging sensor. Section 3.2 explains the pixel array block. Section 3.3 describes the analog readout that reads the information from the pixel array. Section 3.4 explains bias block that generates required biases for analog readout. Section 3.5 describes addressing blocks, and Section 3.6 explains the controller block that generates all digital signals for the sensor.

3.1 Introduction

This section of the thesis gives brief information about CMOS image sensors. Also this section explains the application areas of the designed image sensor. Almost all of the CMOS image sensors have similar main blocks that are required for basic operation.

Figure 3.1 shows the architecture and the floor plan of the imaging sensor. The first block of this image sensor is pixel array. This block is responsible for sensing the object. For this purpose, a detecting part and its reading circuitry exist in this block. Second block is responsible for the selection of each single pixel in the pixel array block. This block is generally formed by row and column selector blocks, and in this thesis, they are called as row and column scanners. Third block processes the output data of each pixel, and gives this data to the output of the chip. This block is called as analog readout. Last block is necessary to generate the signals that are required for pixel array, scanners, and analog readout which is called as controller block. In this thesis, a bias block is added to the system to generate required bias inputs to analog readout

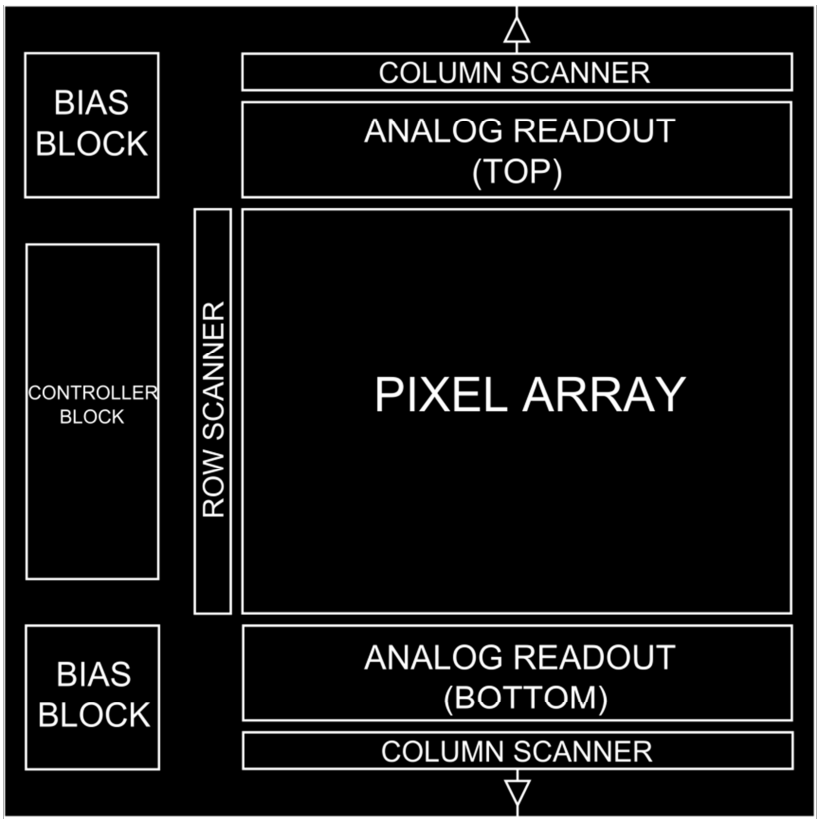

Figure 3.1: Architecture and floor plan of the imaging sensor.

General purpose of the system is to give the information coming from the pixel block to the output. This information, in the scope of this thesis, is the incoming light. In the shadowing method, visible light is going to be detected. In the fluorescence UV imaging method, UV light is going to be detected. This designed chip provides the opportunity of detecting cells using both methods. The chip can be optimized with a few modifications for the desired type of detection technique. In the following sections, these modifications and the function of each block will be explained. The working principles and the simulation results of each block will be presented.

3.2 Pixel Array

Figure 3.2 shows the overall configuration of the pixel array. Pixel array consists of 20480 unit pixels which are arranged in 160×128 format.

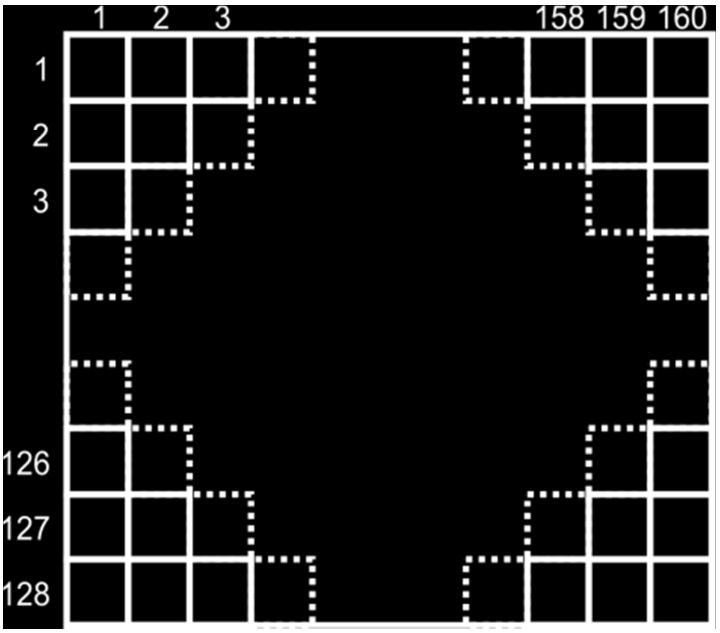

Figure 3.2: Overall configuration of the pixel array.

Figure 3.3 shows the single pixel structure for both DNA and cell detection functions. This block is responsible for converting incoming optical or electrical information to meaningful electrical data. The main function of this pixel array is to detect the signal coming from the sample, and convert it to an electrical signal. This incoming signal can be electrons or photons for this structure. For the DNA detection case, electrons that are revealed due to the hybridization of DNA strands are the incoming signals for the detectors [9]. For the cell detection case, photons coming along the cell samples which are illuminated by a light source are the incoming signals for this block. Thus, to meet both of these functions, two separate detector structures are present in this block.

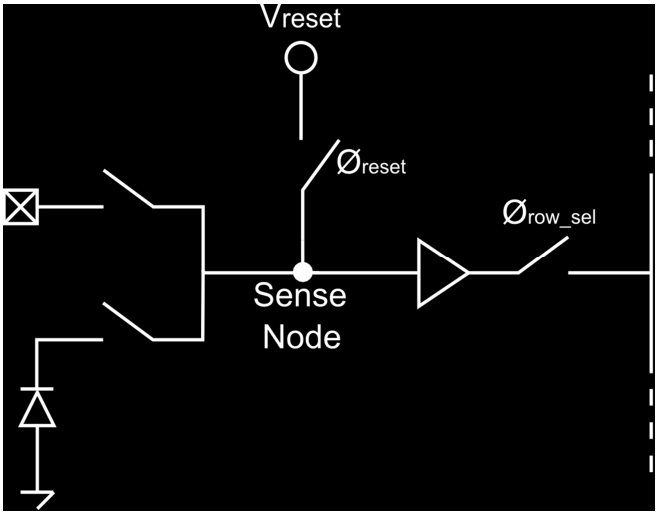

Figure 3.3: Single pixel structure for both DNA and cell detection functions.

In Figure 3.3, sense node is connected to two detector structures via two separate switches. Only one detector structure will be connected to the sense node. The upper detector consists of top metal layer of the process. This metal part can be used to conduct electrons to sense node as used in DNA detection application. Another use of this part is that this metal can be coated with any material for several purposes. For example, to immobilize antibodies in order to hold specific cells on this node, this structure can be used. For this application, the switch that connects this metal to the sense node is off. The lower detector is a photodiode that converts photons to

electrons. This photodiode can be used to transfer the incoming light information to the sense node. Captured cells by immobilized antibodies can be used for optical detection with these photodiodes. As another example, if the fluorescence UV imaging method is used, only the photodetector part is enough. There is no need for immobilization in this case, so the metal layer connected to the sense node is not used, and for this application the upper detector part can be removed. For detection of a specific wavelength light, the process of the fabrication can be optimized (i.e. opto processes). For example photodiode area can be processed to sense light at specific wavelengths. Figure 3.4 shows the top view illustration of single pixel layout.

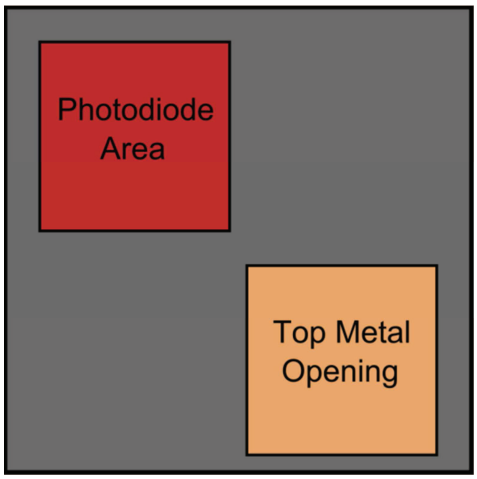

Figure 3.4: Top view illustration of single pixel layout.

The photodiode area is enlarged compared to the sensor that is used for cell detection tests explained in Chapter 2. Since the cell detection technique that is used in the scope of this thesis is lensless, fill factor plays important role for the imaging sensor. Fill factor is the ratio of photosensitive area to the total pixel area. In this design fill factor is increased to 11% from 9%. This means the sensitivity of the sensor to the incoming light is improved by 22%. Also in this thesis, the sensor array format is increased to

160×128 from 32×32, which means the total detector count is increased by 20 times. This increment will allow detecting larger number of cells.

The second aim of this block is to read the sense node. There will be a charge accumulation from the detectors, and voltage resulting from this charge is read out by this block. This reading starts with setting the sense node to a known V_{reset} voltage. This V_{reset} voltage is given via a switch to the sense node. After setting the sense node to a known voltage, this voltage is read first as a reference which means giving this voltage to the output. The switch is placed to off position, and any detector of interest is connected to the sense node via its related switch. This connection would change the voltage of the sense node due to the charge accumulation from the detectors. Then again, the changed voltage is read. The difference of this voltage from the V_{reset} voltage is the information that is taken from the detector. This difference is taken with a software code, not taken with a circuit in the chip.

V_{reset} voltage is set to a maximum voltage, 2.5V, in order to guarantee that the reset transistor is always ON ($V_{GS}>V_{th}$). This voltage must be set to a value as high as possible because when the light comes to the detector, it lowers the sense node voltage so to maximize the voltage swing, V_{reset} is set to a maximum possible voltage, 2.5V. The lower voltage point of the sense node is determined by the analog readout block, which is connected to the output of the pixel block. This voltage is 1.1V, and will be explained in next section, so the pixel can read the voltages between 2.5V and 1.1V which means that voltage swing of the sensor is 1.4V.

3.3 Analog Readout

The main goal of the analog readout block is to transfer the meaningful information coming from the pixel array to out of the chip. This information is the pixel output voltage. When $Ø_{row\_sel}$ signal comes to a row of the array, all the pixel output voltages are transferred to the input of the related column readout circuit. Therefore, for each column of the pixel array, a column readout is available. Then, each voltage at the end

of the column readout is selected with column scanner block, and given to the output driver sequentially.

Figure 3.5 shows simplified architecture of the analog readout block. There is one column readout for each pixel column, and they are connected to a single bus which connects them to the output driver. The voltages are given to the single line with column scanner which will be explained later.

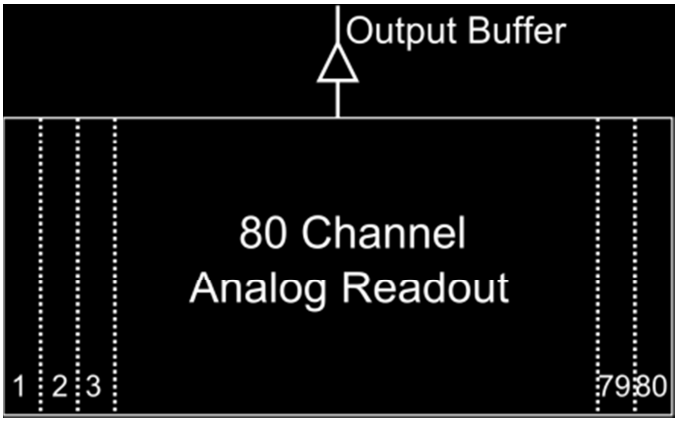

Figure 3.5: Simplified architecture of the analog readout block.

Figure 3.6 shows column readout structure. Column readout is the first stage of the analog readout block. Column readout receives the input signal from the selected pixel array row, and processes till single line bus.

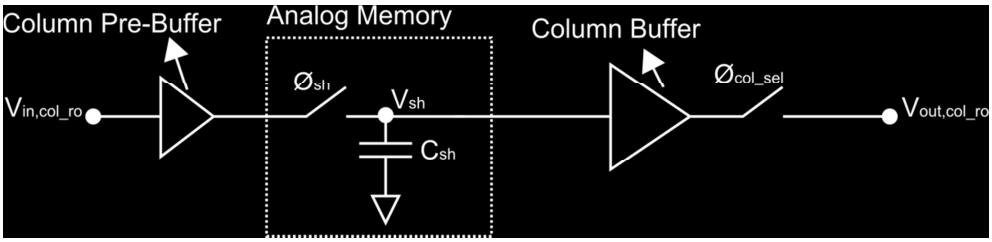

Figure 3.6: Column readout structure.

Column pre-buffer is used to drive the analog memory capacitor with the pixel output voltage. The voltage output of the first buffer stage is held in an analog memory via $Ø_{sh}$ switch. This stage is also called as analog memory. The information coming from the pixel is held in the analog memory capacitor until the next pixel information comes. The stored voltage in the capacitor has to be transferred to the common bus. The output of the analog memory is connected to a common bus using the common buffer circuitry, which prevents signal loss due to a possible charge sharing that would occur if direct connection were used. The column buffer is a one-stage opamp designed to drive the internal capacitive load of the common bus [27]. There are two main jobs of this driver. It transfers its input voltage to the output with a gain that close to unity. To achieve a gain value as close as to unity, the gain of the opamp is designed as high as possible [27].

The second aim of the opamp is to drive its load in a proper time, and the one-stage opamp topology is suitable for this purpose. The main goal is to detect rare cells in the sample which can be done at moderate scanning speeds. At the end of the column buffer, a switch connects the opamp to the common bus, which is controlled by the column scanner.

The last stage of the analog readout block is the output buffer part. Output buffer has a folded cascode opamp topology [27] which can drive large external loads with good stability at the expense of increased power dissipation.

Figure 3.7 shows column readout simulation result. Simulation is done with the single pixel connected to the single column readout. The simulation is done with changing the sense node voltage arbitrarily in the appropriate voltage swing interval of the pixel structure and reading this voltage. The upper first graph belongs to the sense node voltage of the pixel. When $Ø_{row\_sel}$ signal comes, the voltage at this instant is transferred to the column readout which is 1.5V. With the $Ø_{sh}$ signal, this voltage is registered to the analog memory which is the sample and hold capacitor. With the $Ø_{col\_sel}$ signal, this voltage is transferred to the common line bus with a 2mV drop (V_{out}). This drop is due to the column buffer opamp because V_{out}/V_{in} cannot reach 1 even if the gain of the opamp is very high.

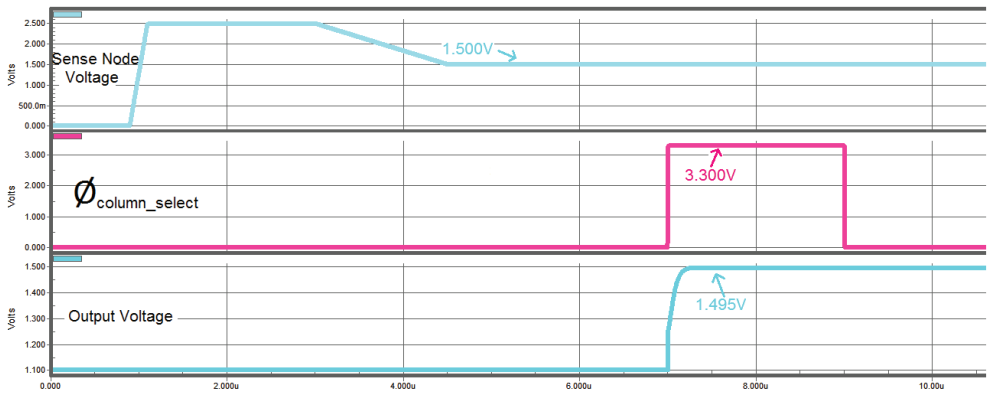

Figure 3.7: Column readout simulation result.

Another critical point about the column buffer is its transient behaviour. The column buffer driving strength determines the frame rate of the sensor because the slowest block in the analog readout is the line column buffer block due to the fact that it drives a large line bus capacitance. All the column bufferss in every column readout is active while the sensor is running so the current drawn from the column buffer should be minimized. A single stage opamp is used as column buffer in this design. Frame rate of the sensor can reach up to 50 frame per second (fps) which is highly enough for cell detection applications since there is no parameter changing with this rate.

The last section of the analog readout block is the output buffer which is implemented using a folded cascode opamp. The output buffer is used to be able to drive large sensor output loads. For noise issues a large capacitance is necessary at the end of the output driver so high current must be drawn from the output driver. Since only two output drivers are used for the sensor architecture, folded cascode topology is suitable for this purpose. The gain of this opamp is higher than the single stage opamp [27] so the error of this opamp is expected to be lower.

The voltage output of the output driver can be digitized using Analog-to-Digital Converter (ADC). The designed sensor has a simulated output noise of 150 μV_{rms}, for an output swing of 1.4V. This noise result corresponds to a dynamic range of 79.4dB,

which shows that this sensor can be used with an ADC having a resolution of 13-bits or better.

3.4 Bias Block

Figure 3.8 shows bias block architecture. Bias block supplies the required bias currents for the analog readout in the sensor. The main idea behind this block is mirroring the main current generated in the chip [27].

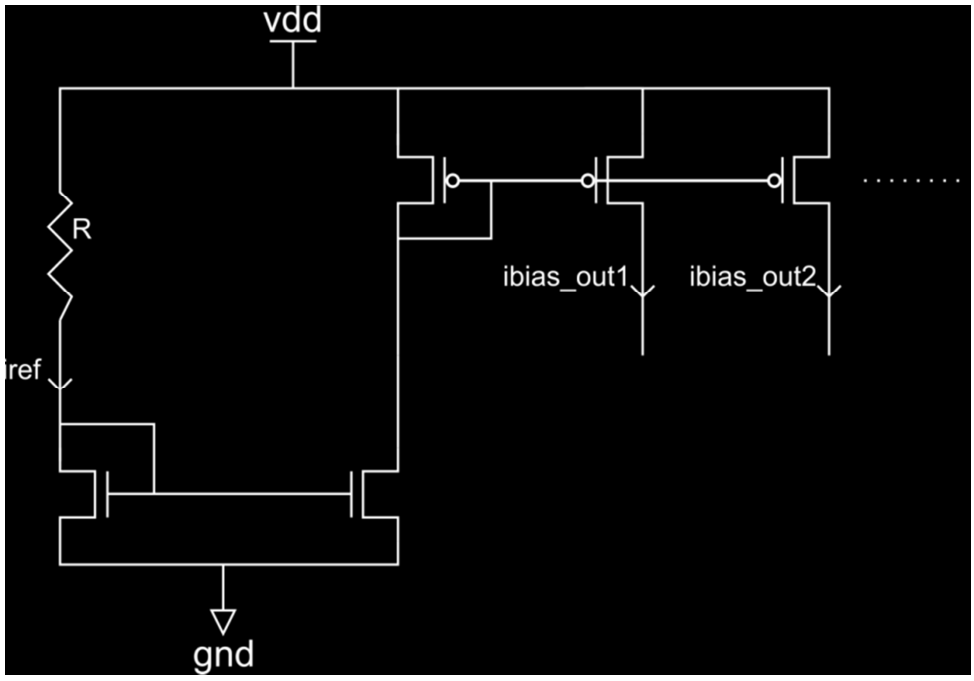

Figure 3.8: Bias block architecture.

The main current is generated with a resistor connected in series between the supply and the diode connected transistor. The design is started with defining a reference current that will be passed through the resistor bank. The drain voltage of the diode connected NMOS transistor is found from to the formula:

$$I_n = \frac{1}{2} K_n \left(\frac{W}{L}\right) (V_{GS} - V_{TN})^2 \qquad [27] \qquad 2.4.1$$

Since, V_{GS} voltage is equal to the drain voltage of the NMOS transistor, V_{GS} is equal to:

$$V_{GS} = \sqrt{\frac{2I_n}{K_n(W/L)}} + V_{TN} \qquad [27] \qquad 2.4.2$$

After setting the drain voltage, the resistor value can be calculated from Ohm's Law. The calculated resistor value supplies the required current in the ideal case however due to process variations, the actual value may differ from this calculated value.

The generated current is mirrored with another NMOS transistor to the PMOS transistors and mirrored one more time with proper scaling factor required by different blocks in the chip. To avoid any possible current adjustment problems, a dedicated external current reference input pad is used (ext_input_cur), along with the test pad called "current_test", allowing to measure the exact value of the generated current in the chip.

3.5 Addressing Blocks

Addressing blocks are designed to address the pixel that is intended to be read. Figure 3.9 shows the schematic diagram of the row scanner block. Pixel array can be thought as 2-dimensional array, and each of its pixels has to be read one by one. The reading is done by selecting a row of the array first. When a row is selected, all of the pixels in this row are meant to be selected. The block that scans each row is called row scanner.

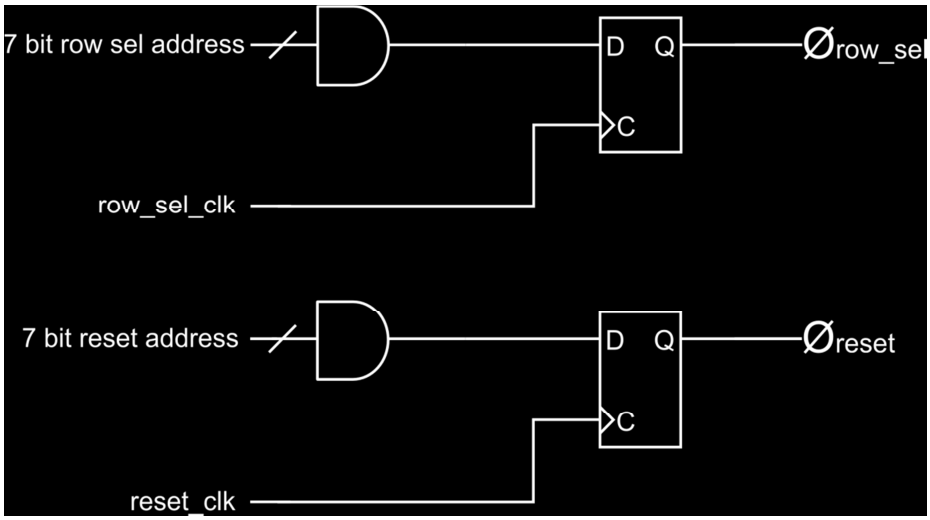

Figure 3.9: Schematic diagram of the row scanner block.

Figure 3.10 shows simulation result of row scanner block. Since there are 128 rows in pixel array, 7 bit addressing will be enough to select each row. The row scanner includes two separate parts. The first part is used for giving the sense node data to the analog readout so it generates $Ø_{row\_sel}$ signal. Second part is used for resetting the sense node, and it generates $Ø_{reset}$ signal. The structures of both parts are identical. When the related address comes from the digital block to the scanners, the output of the AND gate becomes logic 1. The output of the gate is connected to a D-flip-flop. The operation principle of D-flip-flop is such that, it samples the data at the D node to the output (Q) at every positive edge of C signal. This part of this block behaves like a digital memory element. The D-flip-flops generate the row signals required for row selection and row resetting operation at every edge of the applied clock pulse to their C inputs.

There is a delay between row select and reset signals, and this delay corresponds to the exposure or integration time that passes between the removal of reset pulse and beginning of row select pulse used for pixel readout.

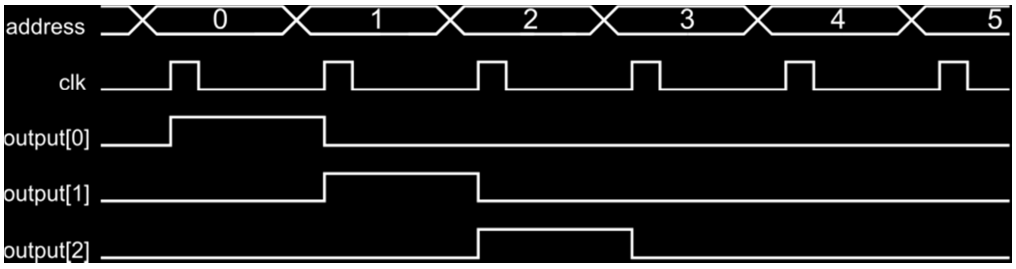

Figure 3.10: Simulation result of row scanner block.

Figure 3.11 shows the column scanner block. Second addressing block is the column scanner block, and this block is similar to the row scanner block.

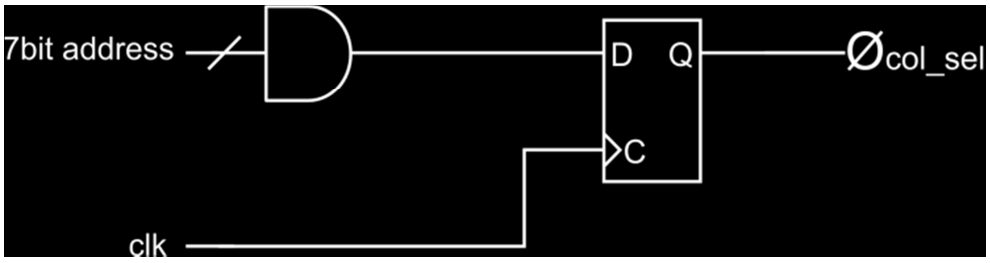

Figure 3.11: Column scanner.

In this block, 7bit addressing is needed since there are 160 columns of pixels in the pixel array. The operation principle is the same with the row scanner block. The output of this block allows each of the column buffer voltage to pass to the common bus so the outputs of this block are generated sequentially.

The advantage of this type of scanners is that addressing can be done. Any pixel that is intended to be read can be read by this type of scanners. Also, array format can be adjusted according to the speed concerns or cell dimension that is targeted to be detected. The cell count problem in Chapter 2 can be solved with reading any desired pixel with this type of scanners. Thus, every single pixel will correspond to a single cell. The advantage here is that there will be no need to post-process the sensor image.

3.6 Controller Block

This block generates the required digital signals for bias block, addressing blocks, and analog readout block. All the configuration settings implemented in the sensor is controlled by the stored bits in the memory block of the controller. The data written to the memory unit is transferred to the switches of different blocks of the sensor, such as the pixel and biasing blocks.

The second function of the controller block is generating the addressing and clock signals of row and column scanner blocks. There is one additional signal in the analog readout called $\emptyset_{sh}$, and this signal is also generated in this block.

Figure 3.12 shows the input and output configuration of controller block. There are four input data entry for the whole controller unit. These inputs are given from four pads of the chip.

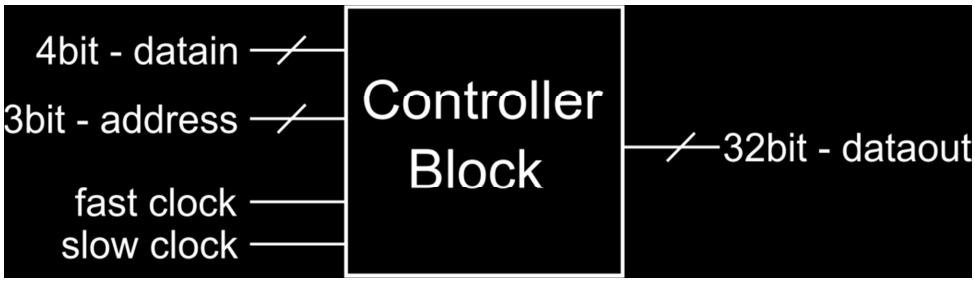

Figure 3.12: Input and output configuration of controller block.

Figure 3.13 shows the single unit of the controller block. These four parallel inputs are given to the first part of the sub-block with a fast clock because there are several of this sub-block present in the controller block. The number of this sub-block is determined by how many signals are required for the other blocks, and every sub-block has an address that selects that sub-block. With the fast clock, all the input data are registered to the first part of the sub-block.

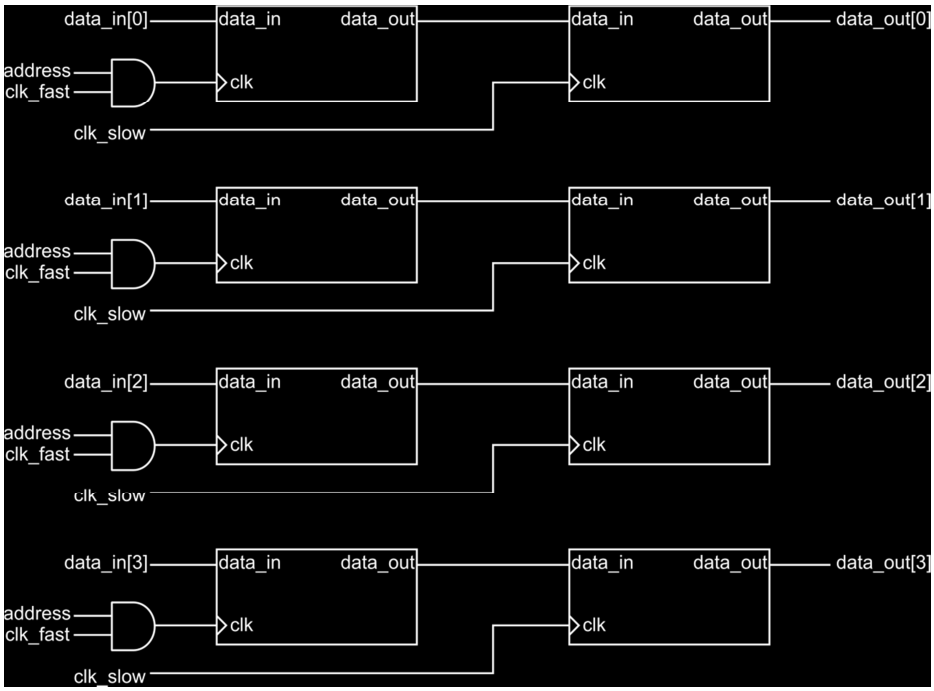

Figure 3.13: Single unit of controller block.

The second part of the sub-block is activated with a slower clock compared to the fast clock. The frequency of this clock has to be as much as the fastest signal that will be delivered to the chip. If the frame rate of the chip is thought to be reaching 50fps, the fastest signal in the chip can be calculated as:

$$\frac{1}{50} \times \frac{1}{128} \times \frac{1}{80} = 1.95\mu s \qquad 2.6.1$$

So, 500 KHz frequency would be enough for the slow clock. Then the faster clock frequency would be the number of sub-block times slow clock.

The advantage of this design is that the required signals for the chip can be adjusted from out of the chip. The duration of reset, row select and column signals can be adjusted, photon integration time can also be adjusted by giving proper delay between reset and row select signals. Additionally, the column select signal, sample and hold signal, and their relative positions among themselves can be adjusted with the help of this controller block.

Figure 3.14 illustrates the proper timing scheme for the proper operation of the sensor which is generated by controller block.

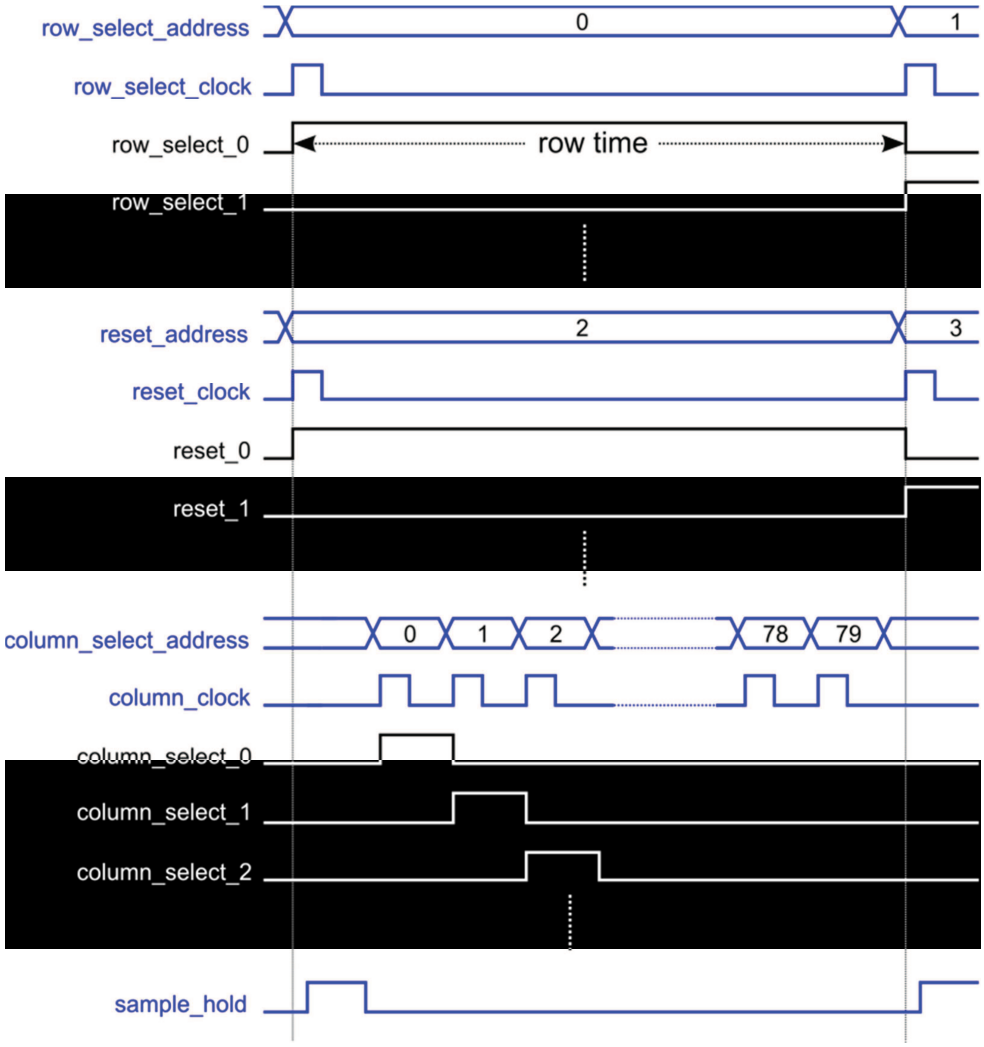

Figure 3.14: Simulation result of the whole digital signals (Blue colored signals are the outputs of controller block).

First of all, resetting of sense node is done. Resetting of 0^{th} row is not shown in Figure 3.14 because while reading the sense node voltage of 0^{th} row pixels, reset signal has gone to 2^{nd} row to reset the 2^{nd} row. After falling to logic 0, again integration of 2^{nd} row begins, and reading will be done when row select signal comes to 2^{nd} row. This

simulation shows reading the 0th row of all 79 column circuits. After some time, when row select signal of the 0th row (row_select_0) becomes high, sampling of the pixel voltage is done with "sample_hold" signal. With dropping this signal, every column voltage of the 0th row is transferred to the common bus and output driver. This is done by closing the switch at the end of the column buffer by column_select signals.

Table 3.1: Unique package pin list of the chip.

Pad Number	***Pad Name***	***Function***	***Pad Number***	***Pad Name***	***Function***
1	address[0]	Digital In	9	datain[0]	Digital In
2	address[1]	Digital In	10	datain[1]	Digital In
3	address[2]	Digital In	11	datain[2]	Digital In
4	clock	Digital In	12	datain[3]	Digital In
5	reset	Digital In	13	ext_input_cur	Analog In
6	vdd	Power	14	current_test	Analog Out
7	vss	Ground	15	anolog_output[0]	Analog Out
8	memory	Digital In	16	analog_output[1]	Analog Out

Table 3.2: Comparison of the features of the newly designed sensor with the previous work.

	Previous Work	***This thesis***
Cell Detection	✓	✓
DNA Detection	-	✓
Array Format	32×32	160×128
Fill Factor	9%	11%
Dynamic Range	1.14V	1.40V
Address based scanners	-	✓
On chip output driver and bias circuitry	-	✓
Ripple Mode	-	✓

The sensor chip runs at 3.3V supply voltage. It has 42 pads, most of which are multiple power and ground pads. The sensor can be operated using only 16 unique pins after combining common power and ground inputs. Table 3.1 shows unique package pin list of the chip, and Table 3.2 shows comparison of the features of the newly designed sensor with the previous work. Figure 3.15 shows the layout of the designed image sensor. The chip measures 4.1mm(H) × 4.4mm(V) in a 0.35µm CMOS process.

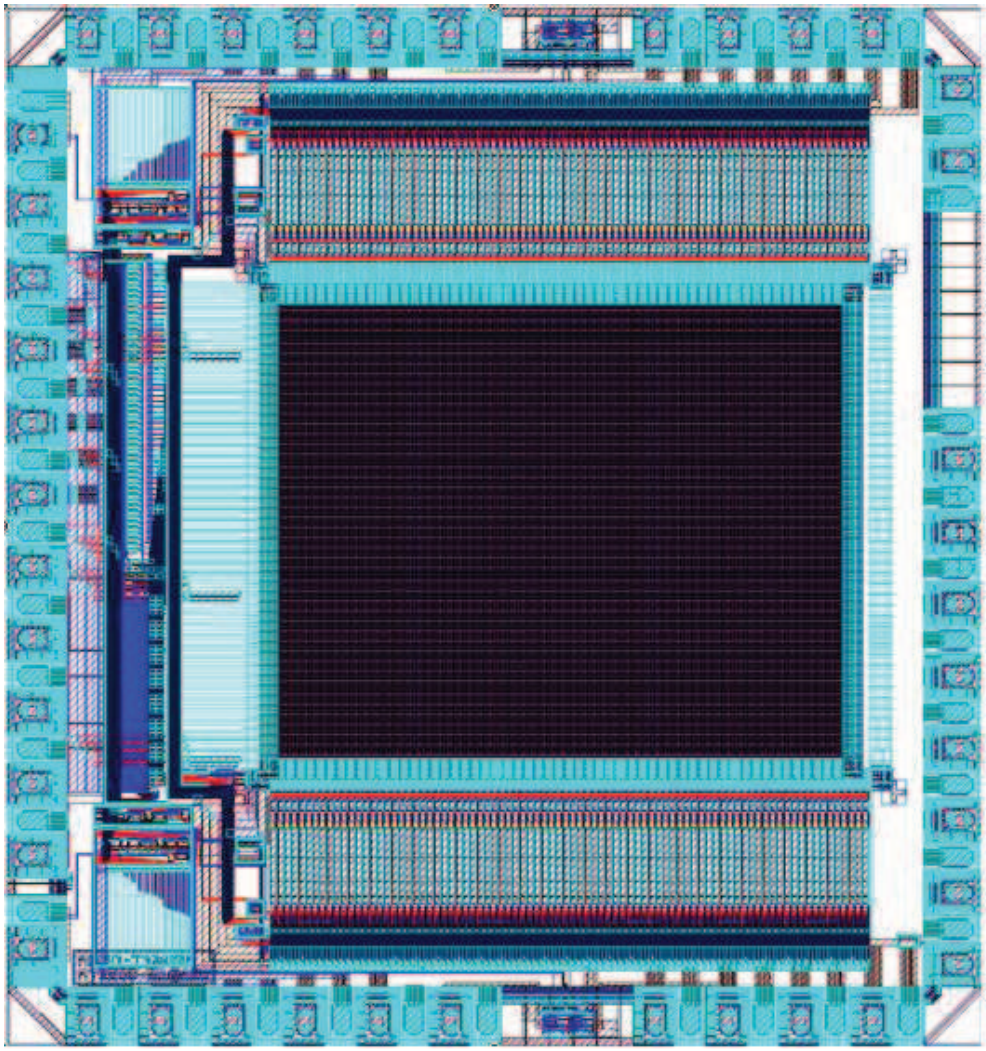

Figure 3.15: Layout of the designed image sensor. The chip measures 4.1mm(H) × 4.4mm(V) in a 0.35µm CMOS process.

CHAPTER IV

CONCLUSIONS AND FUTURE WORK

In the scope of this thesis, two separate studies are done. First of all, an image sensor that is designed in METU-MEMS Research and Application Center is used for cell detection tests to see if it is useful for cell detection purposes. The tests are done with baker's yeast cells, dried in PBS solution, and it is seen that even a single yeast cell can be detected with this sensor. The sensor image is processed, and contrast is increased with an algorithm. With this image processed result, cells appear more distinctive than the unprocessed result.

After getting successful results with yeast cells, tests are performed with breast cancer (MCF-7) cells in PBS. First, cells are placed in PBS solution, and sensor image is taken for three different cases of PBS solution. The best results are taken when the solution is about to dry. Because the liquid blocks the incoming light, and prevents the formation of shadows on the sensor, or the cells are placed above the sensor surface, and the sensor cannot get images without cells placed zero distance from the sensor surface.

To answer this question, and even more, the sensor surface is coated with gold electrolessly in order to bind antibody to the sensor surface. After coating gold, anti-P-glycoprotein is bound to the gold surfaces of the sensor. This is the antibody of the drug resistant MCF-7 cells because drug resistant MCF-7 cells have P-glycoprotein around them. Drug resistant MCF-7 cells did not bound to the antibody immobilized sensor surface in the first tests. The reason why they did not bound to the antibodies

was the preparation method of the drug resistant MCF-7 cells. These cells usually bound to the surfaces of their growth medium (flask) while they are growing, and the biologists usually separate the cells from the surfaces of these flasks with using trypsin enzyme. When the cells are separated from their flask surfaces without using trypsin enzyme, the cells bound to their antibodies. Most probably, the reason why the first cells did not bound to the antibodies was because of the use of this enzyme. After successful binding, again cells are not sufficiently detected while they are in the PBS solution, and the same cells are detected while the solution is about to dry. This brings the conclusion that with this method, cell detection only occurs in the absence of any fluidic solution. The only way of detecting living carcinogenic cells is getting the sensor image when the medium or solution is about to dry.

It is seen from the images that the sensor can be improved, and an advanced version of this sensor is designed. The basic architecture of the pixel circuit is not changed but a diode is added to each pixel instead of the source diffusion area of the reset transistor. With this modification, improvement in the fill factor achieved, and thus, better sensitivity is expected relative to the used sensor. Additionally, a top level metal is also kept available which is connected to the sense node of the pixel circuit with a switch. This metal has a passivation opening on it for several purposes. With coating gold on this metal, specific cell binding can be done for rare cell detection applications. Moreover, DNA detection can also be done with this structure.

In the new design, pixel addressing is done so that even any desired single pixel can be investigated, and the cell presence in this pixel can be viewed. The pixel number is also increased in order to see more cells in the samples. The first design has a pixel array of 32×32 resulting 1024 pixels on it whereas the new designed chip has a resolution of 160×128 resulting 20480 pixels on it. Although more pixels are present in the new design, with the addressing capability of the scanners, array format can be changed for detection of bigger size cells. In this design, all the biasing is done inside the chip, and no external biasing is required. Finally, an output buffer is placed inside the chip so that the sensor chip can drive external loads easily without any external buffer circuit.

As future work, the following items can be studied or performed:

1. The sensitivity of the sensor can be tested at different wavelengths to determine the spectral response of the sensor.
2. Specific antibodies to the specific cancer cells can be bound to the sensor. Following that, a mixture of different cancer or different living cells can be exposed to that sensor, and try to observe that, after multiple washings, the desired cancer cells are still bound to the sensor surface.
3. The tests explained in thesis can be repeated using the newly designed sensor after its fabrication.
4. UV fluorescence imaging can be investigated in detail. With some post processing, specific wavelengths coming from the cell samples can be detected in order to see carcinogenic tissues.
5. DNA detection tests can also be performed using the newly designed sensor chip.

REFERENCES

[1] Z. Darzynkiewicz, J. P. Robinson, and H. A. Crissman, Methods in Cell Biology, Academic Press, 1994.

[2] S. S. Saliterman, Fundamentals of BioMEMS and Medical Microdevices, SPIE Press, 2005.

[3] A. Fuchs, N. Manaresi, D. Freida, L. Altomare, C. L. Villiers, G. Medoro, A. Romani, I. Chartier, C. Bory, M. Tartagni, P. N. Marche, F. Chatelain, and R. Guerrieri, "A Microelectronic Chip Opens New Fields in Rare Cell Population Analysis and Individual Cell Biology," 7th International Conference on Miniaturized Chemical and Biochemical Analysis Systems, pp. 911-914, 2003.

[4] N. Manaresi, A. Romani, G. Medoro, L. Altomare, A. Leonardi, M. Tartagni, and R. Guerrieri, "A CMOS Chip for Individual Cell Manipulation and Detection," IEEE International Solid-State Circuits Conference, 2003.

[5] T. Tam, G. A. Jullien, and O. Yadid-Pecht, "A CMOS Contact Imager for Cell Detection in Bio-Sensing Applications," Proceedings of IEEE ISCAS, New Orleans, LA, USA, pp. 813-816, 2007.

[6] D. Rosenbaum, S. D. Girouard, and K. R. Laurita, "High Resolution Cardiac Mapping with Voltage Sensitive Dyes." Proceedings of the Annual International Conference of the IEEE Engineering in Medicine and Biology Society, vol. 5, pp. 1995-1996, 1992.

[7] C. Stagni, C. Guiducci, L. Benini, B. Ricco, S. Carrara, B. Samori, C. Paulus, M. Schienle, M. Augustyniak, and R. Thewes, "CMOS DNA Sensor Array With Integrated A/D Conversion Based on Label-Free Capacitance Measurement," IEEE Journal of Solid State Circuits, Vol. 41, No. 12, pp. 2956-2964, 2006.

[8] D. S. Kim, Y. T. Jeong, H. J. Park, J. K. Shin, P. Choi, J. H. Lee, and G. Lim, "An FET-Type Charge Sensor for Highly Sensitive Detection of DNA Sequence," Biosensors

and Bioelectronics, Vol. 20, pp. 69-74, 2004.

[9] J. Musayev, "CMOS Integrated Sonsor Readout Circuitry for DNA Detection Applications," Middle East Technical University, 2011

[10] T. Tanaka, T. Saeki, Y. Sunaga, and T. Matsunaga, "High-content analysis of single cellls directly assembled on CMOS sensor based on color imaging." Biosensors and Bioelectronics, Vol. 26, pp. 1460-1465, 2010.

[11] S. Seo, T. W. Su, D. K. Tseng, A. Erlinger, and A. Ozcan, "Lensfree holographic imaging for on-chip cytometry and diagnostics," Lab Chip, Vol. 9, pp. 777-787, 2009.

[12] A. Ozcan and U. Demirci, "Ultra wide-field lens-free monitoring of cells on-chip," Lab Chip, Vol. 8, pp. 98-106, 2008.

[13] Y. Hosseini and K. V.I.S. Kaler, "Integrated CMOS optical sensor for cell detection and analysis," Sensors and Actuators A: Physical, Vol. 157, pp. 1-8, 2010.

[14] A. Richards, "Digital Reflected - Ultraviolet Imaging," Advanced Imaging Magazine, April 2006.

[15] D. S. Ferreira, M. Henriques, R. Oliveira, J. H. Correira, and G. Minas, "Autofluorescence Spectroscopy of a Human Gastrointestinal Carcinoma Cell Line: design of optical sensors for the detection of early stage cancer," Proceedings of the International Conference on Biomedical Electronics and Devices, pp. 61-66, 2009.

[16] R. A. Dias, J. H. Correia, and G. Minas, "On-Chip Integrated Optical Sensors for Fluorescence Detection of Cancer Tissue: Application to Capsule Endoscopy," Proceedings of ICECS-The 14th International Conference on Electronics, Circuits and Systems, pp. 423-426, 2007.

[17] R. A. Dias, J. H. Correia, and G. Minas, "CMOS Optical Sensors for being incorporated in Endoscopic Capsule for Cancer Cells Detection," Proceedings of ISIE, pp.2747-2751, 2007.

[18] G. Minas, J. C. Ribeiro, R. F. Woffenbuttel, and J. H. Correia, "On-Chip Integrated CMOS Detection Microsystem for Spectrophotometric Analyses in Biological Microfluidic Systems," Proceedings of ISIE, pp. 1133-1138, 2005.

[19] G. Minas, J. S. Martins, J. C. Ribeiro, R. F. Wolffenbuttel, and J. H. Correia, "Biological Microsystem for Measuring Uric Acid in Biological Fluids," Sensors and Actuators, Elsevier, vol.110, pp. 33-38, 2004.

[20] P. E. Gray and C. L. Searle, Electronic Principles: Physics, Models and Circuits, John Wiley & Sons, Inc., 1969.

[21] M. Teymouri, Kh. Hadidi, and A. Khoei, "A New Linear Readout Circuit for a CMOS Image Sensor," European Conference on Circuit Theory and Design, pp. 213-216, 2009.

[22] J. Janesick, F. Gunawan, T. Dosluoglu, J. Tower, and N. McCaffrey, "Scientific CMOS Pixels," Experimental Astronomy, Vol. 14, pp. 33-43, 2002.

[23] A. Rogalski, K. Adamiec, and J. Rutkowski, Narrow-Gap Semiconductor Photodiodes, SPIE Press, 2000.

[24] P. V. Kasperkovitz, N. S. Khan, J. M. Tam, M. K. Mansour, P. J. Davids, and J. M. Vyas, "Toll-Like Receptor 9 Modulates Macrophage Antifungal Effector Function during Innate Recognition of Candida alnicans and *Saccharomyces cerevisiae*," Infection and Immunity, Vol. 79, pp. 4858-4867, 2011.

[25] H. Boulaiz, J. Prados, C. Melguizo, A. M. Garcia, J. A. Marchal, J. L. Ramos, E. Carrillo, C. Velez, and A. Aranega, "Inhibition of Growth and Induction of Apoptosis in Human Breast Cancer by Transfection of Gef Gene," British Journal of Cancer, Vol. 89, pp. 192-198, 2003.

[26] K. L. Mealey, R. Barhoumi, R. C. Burghardt, S. Safe, and D. T. Kochevar, "Doxycycline Induces Expression of P Glycoprotein in MCF-7 Breast Carcinoma Cells," Antimicrobial Agents and Chemotherapy, Vol. 46, pp. 755-761, 2002.

[27] B. Razavi, Design of Analog CMOS Integrated Circuits, McGraw-Hill, 2001.